Taylor & Francis
Taylor & Francis Group

Science and Technology for the Built Environment

ISSN: 2374-4731 (Print) 2374-474X (Online) Journal homepage: http://www.tandfonline.com/loi/uhvc21

Performance investigation of nano-structured composite surfaces for use in adsorption cooling systems with a mass recovery cycle

L.Q. Zhu, C.Y. Tso, K.C. Chan, C.L. Wu, J. Chen, W. He, S.W. Luo & Christopher Y.H. Chao

To cite this article: L.Q. Zhu, C.Y. Tso, K.C. Chan, C.L. Wu, J. Chen, W. He, S.W. Luo & Christopher Y.H. Chao (2018): Performance investigation of nano-structured composite surfaces for use in adsorption cooling systems with a mass recovery cycle, Science and Technology for the Built Environment, DOI: 10.1080/23744731.2018.1479613

To link to this article: https://doi.org/10.1080/23744731.2018.1479613

Accepted author version posted online: 19 Jun 2018.

Performance investigation of nano-structured composite surfaces for use in adsorption cooling systems with a mass recovery cycle

L.Q. Zhu[1], C.Y. Tso[1, 2], K.C. Chan[1], C.L. Wu[3], J. Chen[3], W. He[3], S.W. Luo[3], and Christopher Y.H. Chao[1, *]

[1]Department of Mechanical and Aerospace Engineering, The Hong Kong University of Science and Technology, Clear Water Bay, Kowloon, Hong Kong, China;

[2]HKUST Jockey Club Institute for Advanced Study, The Hong Kong University of Science and Technology, Hong Kong, China;

[3]Buliding Energy Research Center, Guangzhou HKUST Fok Ying Tung Research Institute, Guangzhou, China

Received 09 Mar 2018; accepted 09 May 2018

Christopher Y.H. Chao, PhD.

*Corresponding author e-mail: meyhchao@ust.hk

With an increase of the heat transfer coefficient and condensation rate in a condenser, a lower pressure can be achieved in a desorber, which leads to a dryer adsorber for the next adsorption phase and a better cooling performance in an adsorption cooling system. This study aims to experimentally investigate the condensation rate of different nano-structured surfaces and improve the cooling performance of an adsorption cooling system by coating a superhydrophobic - zeolite 13X adsorbent composite surface in the condenser. An experiment was designed and built to investigate the condensation rate of various nano-structured

surfaces on a copper plate. The results show that a water collection rate (condensation rate) of the superhydrophobic – zeolite 13X adsorbent composite surface of 49.3 g/m^{2}min is achieved, which shows an enhancement of about 50% compared to that of the copper surface. A mathematic model is developed to estimate the cooling performance of the adsorption cooling system utilizing the composite surface and a mass recovery cycle. The simulation results show that a SCP of 231.4 W/kg and a COP of 0.317 are determined, which shows an improvement of 25.0% and 7.8%, respectively, compared to that of the system without coating the nano-structured composite surface.

Nomenclature

A	area, m^2
c_p	specific heat capacity of water, J/(kgK)
COP	coefficient of performance
D	diameter, m
D_{s0}	pre-exponent constant, m^2/s
E_a	activation energy of surface diffusion, J/mol
f	friction factor
ΔH	adsorption heat, J/kg
h_L	heat loss of flow, Pa
K	mass transfer coefficient, 1/s
K_L	loss coefficient
L	latent heat, J/kg
l	length, m
M	molar mass, g/mol
$\dot{m}$	mass flow rate, L/min
N	number
P	pressure, Pa
R	gas constant, J/Kmol
RH	relative humidity, %
r	radius, m
Re	Reynolds number
SCP	specific cooling power, W/kg
T	temperature, ^oC
t	time, s

U	heat transfer coefficient, W/m^{2}K
V	volume, m^3
v	velocity, m/s
W	mass, kg
ε	porosity
λ	equivalent roughness, mm
ρ	density, kg/m^3
ω	water uptake, g/g

Subscripts

adb	adsorbent
ads	adsorption
al	aluminum
c	coated
chw	chilled water
cs	composite surface
con	condenser
crt	testing of condensation rate
cu	copper
cw	cooling water
cycle	cycle
des	desorption
ec	environmental chamber
eq	equilibrium
eva	evaporator

hr	heat recovery phase
hw	hot water
i	inner
in	inlet
ma	maximum
mi	minimum
mr	mass recovery phase
out	outlet
p	particle
pi	pipe
s	saturate
uc	uncoated
v	water vapor
w	water

Introduction

Adsorption cooling systems (ACSs) have drawn attention in the past few decades, because of their low electricity consumption and minimal environmental impact (Akahira et al., 2004). ACSs utilize low-grade heat sources such as waste heat or solar energy to drive the refrigerant cycle (Nidal et al., 2010; Ng et al., 2012). Water can be used as the refrigerant (the adsorbate) depending on the performance of the adsorbent, which is more environmentally friendly, compared with the refrigerant of vapor compression systems (Wang, 2001; Anyanwu, 2004). However, there are still a number of technical challenges, which limit the wide use of the ACSs, such as low efficiency, bulky size, high manufacturing cost, etc. Over recent decades, a lot of studies about ACSs have been proposed and achievements are being made.

The condenser is a major component of an ACS. With an increase of the heat transfer coefficient and condensation rate in the condenser, a lower pressure in the desorber can be achieved, which leads to a larger amount of desorbed water vapor. If more water vapor can be desorbed, the adsorbent will be dryer, so that more water vapor can be adsorbed in the next adsorption phase. Therefore, improving the performance of the condenser can effectively improve the cooling performance and reduce the size of the ACS (Youssef et al., 2015). Currently, most of the studies about the condenser of the ACS were focused on the effect of the cooling water inlet temperature to the condenser on the performance of the condenser (Youssef et al., 2016; Thu et al., 2011). However, the cooling water inlet temperature is not the only factor affecting the performance of the condenser. For example, utilizing finned heat exchangers in the condenser coated with different nano-structured surfaces also shows the potential to enhance the performance of the condenser (Edwards and Doolittle, 1965). It is reported that nano-structured superhydrophilic surfaces (Dong et al., 2017) and nano-structured superhydrophobic surfaces (Lu et al., 2017) for use in dehumidification

systems show an improvement in condensation rate, thus it is believed that they may also have the potential to enhance the cooling performance of the condenser in an ACS.

Dong et al., and Qi et al., developed a liquid desiccant plate dehumidifier coated with a nano-structured TiO_2 superhydrophilic surface. The results showed that enhancing ratios for the moisture removal rate and dehumidification efficiency were 1.6 and 1.63, respectively compared with a dehumidifier without the superhydrophilic surface (Dong et al., 2017; Qi et al., 2016). Cheng et al. numerically investigated the nano-structured superhydrophobic surfaces and reported that the dropwise condensation on the superhydrophobic surfaces showed a superior heat transfer coefficient than that of the filmwise condensation (Cheng et al., 2016). Lu et al. developed a superhydrophobic Si nanowire surface and a condensation heat transfer coefficient of 88 kW/m^2K was achieved, showing an improvement of 155% and 87% compared to that of using conventional hydrophilic and hydrophobic surfaces, respectively (Lu et al., 2017). Apart from nano-structured superhydrophilic surfaces and nano-structured superhydrophobic surfaces, a membrane coated with adsorbents, named an adsorbent membrane, on a superhydrophilic surface or superhydrophobic surface has the potential to enhance the condensation rate. In physical sorption processes, hydrogen molecules will be attracted on the surface of adsorbents due to the van der Waals force between the hydrogen molecules and the adsorbents (Lennard-Jones, 1932). Grzech et al. investigated the effect of van der Waals interactions on hydrogen storage capacity and heat of adsorption of silica-based materials. The results showed that with increasing the pore size, the van der Waals force and hydrogen uptake decrease (Grzech et al., 2014). The van der Waals force affects the movement of the droplets nearby, so that the droplets move towards the adsorbent membrane and the droplets can combine with other droplets on their way to form bigger droplets, which reduce the wettability of the membrane and increase the condensation rate. The van der Waals force also affects the water vapor in the moist air nearby, so that the

humidity of the area close to the composite surface increases, which leads to a higher mass transfer between the composite surface and moist air. However, a composite surface consisting of a superhydrophilic surface, a superhydrophobic surface and adsorbent membranes has not been developed yet. In this study, plain copper surfaces, superhydrophilic surfaces and superhydrophobic surfaces were developed, and superhydrophilic – zeolite 13X adsorbent composite surfaces and superhydrophobic – zeolite 13X adsorbent composite surfaces were invented. The condensation rates on different surfaces were investigated experimentally.

The performance of the integrated unit of the adsorbent and heat exchanger (AdHex) (Aristov et al., 2012), can influence the adsorption capacity and heat and mass transfer of the adsorber, which can affect the coefficient of performance (COP) and specific cooling power (SCP) of the ACSs (Frazzica et al., 2014). Ahmed et al. separated all available adsorbents into three categories, which are physical adsorbents, chemical adsorbents and composite adsorbents (Ahmed et al., 2012). Boelman et al. investigated a silica gel – water adsorption cooling system (ACS) and a COP of 0.4 was obtained with a desorption temperature of 50 °C (Boelman et al., 1995). Wang et al. evaluated ACSs using five different adsorbents and found that although the SCP of the silica gel was not as high as the composite adsorbents, the silica gel was a suitable choice for ACSs driven by low temperature heat sources (50-100 ^{o}C) (Wang et al., 2009). Improving the method of filling the adsorbent material into the adsorbers is one of the choices to enhance the performance of the AdHex. Wang et al. developed and investigated the performance of a fluidized-adsorbent bed. An improvement of the average mass variation rate of the adsorbate of 630% was achieved by using a fluidized adsorbent and fluidized-adsorbent bed compared to the conventional packing in adsorbent beds (Wang et al., 2012). Chan et al. developed and investigated an adsorbent bed consisting of cylindrical shell units which were copper tubes with circular fins covered by stainless metal meshes. The

silica gel was packed in between the circular fins and a SCP of 81.4 W/kg was estimated (Chan et al., 2015). Compared with the packing and fluidizing methods, coating technology can highly enhance the performance of the AdHex (Li et al., 2015). Tatlier developed an adsorbent bed coated with zeolite and with metal-organic frameworks. The results showed that the performance of the adsorbent bed coated with metal-organic frameworks were 4-5 fold higher than that coated with zeolite under a desorption temperature of 110 ^{o}C (Tatlier, 2017). However, the cost of using most of the coating technologies was usually higher and the preparation of the coating technologies was usually more complicated than that of packing technologies. An electrostatic coating method which is low in cost and fast in preparation, has the potential to be utilized in coating the adsorbent on the adsorbent beds (Zhu et al., 2018). The electrostatic coating has four major advantages. 1) The adsorbent particles can be sprayed all over the adsorbent membrane because of the combination of mechanical and electrical forces, so that the adsorbent on the adsorbent membrane is evenly distributed (Yang et al., 2017). 2) The coating adsorbents on the membranes can be well-confined and the thickness of the coating can be well-controlled (Luo et al., 2008). 3) The electrostatic coating method does not affect the properties of the adsorbent passing through the spray gun (Prasad et al., 2016). 4) The preparation of the adsorbent membrane using electrostatic coating is fast and low in cost (Zhu et al., 2018).

In terms of application, the operating parameters and operating sequences will affect the performance of the ACS (Sapienza et al., 2011; Chan et al., 2015). Miyazaki et al. developed a novel dual evaporator typed adsorption chiller with three adsorbent beds and tested the effect of operating temperatures and cycle time on the SCP and COP. It was found that the higher the chilled water inlet temperature, the higher the SCP and COP (Miyazaki et al., 2010). Tso et al. simulated the effect of adsorption/desorption phase time, hot water inlet temperature, cooling water inlet temperature and chilled water inlet temperature on the SCP

and COP. The results showed that these parameters had a great influence on the SCP and COP, although the chilled water inlet temperature only showed a significant effect on the SCP (Tso et al., 2012). Besides, Tso et al. also experimentally studied various operating sequences and proposed a pre-cooling and pre-heating cycle. A SCP and COP of 106 W/kg and 0.16 were achieved, which were 129% and 100% increases respectively compared to the basic cycle (Tso et al., 2015). In our previous study, Zhu et al. developed and investigated an advanced mass recovery phase for a double-bed ACS. During the advanced mass recovery phase, two adsorbers and the condenser are connected, while hot water was kept supplying to the desorber and cooling water was kept supplying to the adsorber. A SCP of 180.4 W/kg and COP of 0.29 were achieved after utilizing the advanced mass recovery phase. The results showed that the advanced mass recovery phase significantly improved the cooling performance of the ACS (Zhu et al., 2017). In this study, this advanced mass recovery phase was conducted. Compared with the traditional mass recovery (whereby only two adsorbers are connected to each other), the condenser plays a more important role in the advanced mass recovery phase.

This study aims to develop and experimentally investigate nano-structured composite surfaces for use in a condenser of an ACS, and also to numerically estimate the cooling performance of the ACS after employing the nano-structured composite surfaces. Silica gel-water was used as the adsorbent-adsorbate working pair. In this study, an advanced mass recovery phase, which is detailed described in Section 2.2, was conducted. Five different surfaces including a plain copper surface, nano-structured superhydrophobic surface, nano-structured superhydrophilic surface, nano-structured superhydrophobic – zeolite 13X adsorbent composite surface and a nano-structured superhydrophilic – zeolite 13X adsorbent composite surface were developed and investigated experimentally. The nano-structured superhydrophobic and superhydrophilic surfaces were prepared with the dip coating method

proposed by Larmour et al. (Larmour et al., 2007) since it is one of the most cost- and time-efficient methods (Sun et al., 2014; Traipattanakul et al., 2017). The adsorbent membrane was prepared with the electrostatic coating method and coated onto the nano-structured superhydrophilic surface or nano-structured superhydrophoic surface to form the nano-structured superhydrophilic – adsorbent composite surface or nano-structured superhydrophobic – adsorbent composite surface. More importantly, mathematical models were developed to simulate the cooling performance of the ACS utilizing the nano-structured superhydrophobic – zeolite 13X composite surface in the condenser.

Operating Cycle

Basic Operating Cycle

The basic operating cycle of a double-bed ACS consists of two major phases, named Phase I and Phase II in this study. The two adsorbers are named adsorber A and adsorber B.

In Phase I, adsorber A is in the adsorption process while adsorber B is in the desorption process. The refrigerant (water in this study) rapidly evaporates continuously to produce water vapor and a cooling effect in the evaporator at a low evaporation temperature. The water vapor flows to adsorber A due to the pressure difference. The water vapor is adsorbed by the adsorbent in adsorber A and the low pressure condition is maintained. Cooling water passing through adsorber A removes the heat generated due to the adsorption process. Adsorber B is heated to a desorption temperature by hot water passing through adsorber B. The water vapor is desorbed from the adsorbent in adsorber B and flows to the condenser due to the pressure difference between the adsorber and condenser. Water vapor condenses in the condenser, and flows to the evaporator due to the pressure difference between the condenser and evaporator and the gravitational effect.

Phase II is similar to Phase I, but the adsorbent in adsorber A is heated to desorb while that in adsorber B is cooled to adsorb.

Advanced Mass Recovery Phase

Mass recovery is a common method to improve the performance of the system (Chua et al., 2002). In a traditional mass recovery phase, two adsorbers are connected to each other. Adsorbers perform the desorption process by pressure difference only. However, if hot water continues to be supplied to adsorbers during the mass recovery phase, they can desorb more water vapor since a high desorption temperature can be maintained (Zhu et al., 2017; Zhu et al., 2018). Moreover, if the adsorbers are connected to the condenser, the pressure inside the adsorbers can be further reduced because of the condensation effect, which leads to a better desorption process.

In this study, advanced mass recovery phases, named Phase I-M and Phase II-M, were adopted. Right after Phase I, the pressure of adsorber B is much higher than that of adsorber A. Phase I-M is operated. In Phase I-M, adsorber A and adsorber B are connected to each other, while cooling water continues to be supplied to adsorber A and hot water continues to be supplied to adsorber B. At the same time, adsorber A is connected to the condenser. By connecting the two adsorbers and condenser together, the water vapor flows from the higher pressure adsorber to the lower pressure adsorber and then to the condenser automatically. The water vapor condenses in the condenser, which reduces the pressure. The adsorbers are depressurized. Phase I-M can further dry the heated adsorber after desorption (adsorber B) and reduces the internal pressure. The dryer adsorbent can adsorb more water vapor in Phase II. Right after Phase II, Phase II-M is operated. In Phase II-M, adsorber A and adsorber B are connected to each other and adsorber B is connected to the condenser, while hot water continues to be supplied to adsorber A and cooling water continues to be supplied to adsorber

B. Phase I-M and Phase II-M are completed after the pressure in the two adsorbers and the condenser is balanced, and then a heat recovery phase is operated immediately, named Phase H.

Heat Recovery Phase

In Phase H, the heat transfer fluid (water) flows through adsorber A and B to recover about 30% of the heat input of the desorption phase due to the temperature difference (Li et al., 2009; Qu et al., 2001). Phase H is completed when the temperature of water in the two adsorbers is balanced.

In this study, a complete operating sequence is described as: "Phase I → Phase I-M → Phase H → Phase II → Phase II-M → Phase H → Phase I → ...".

Effect of Conducting the Advanced Mass Recovery Phase on the Cooling Performance of the ACS

In a traditional mass recovery phase, the adsorber and desorber are connected with each other and the water vapor flows from desorber to the adsorber. The pressure in the dsorber is reduced. The desorption process in the desorber is performed by the pressure difference only. In an advanced mass recovery phase, the pressure inside the desorber deceased more rapidly since water vapor flowed from the desorber to the adsorber, and at the same time, water vapor condensed in the condenser, which further reduced the pressure in the desorber. The adsorbent temperature remains constant because of the hot water supply. The constant adsorbent temperature and pressure reduction cause an extra desorption process, leading to a better performance.

Table 1 shows the experimental results of the ACS with different operating cycles. The experiments were conducted with an operating condition of a hot water inlet temperature of 90 ^{o}C, a cooling water inlet temperature of 25 ^{o}C, a chilled water inlet temperature of 16 ^{o}C, a hot water flow rate of 8 L/min, a cooling water flow rate of 8 L/min, a chilled water flow rate of 2 L/min, an adsorption/desorption phase time of 660 s, and a heat recovery phase time of 50 s. For the traditional mass recovery phase (TMR), the best performance of the system occurred when it was conducted for 15 s. After conducting the traditional mass recovery phase and heat recovery phase (HR), the SCP increased by 17.5% compared to that of the basic operating cycle (BC). After conducting the advanced mass recovery phase (AMR) with an optimized time of 85 s, the SCP increased by 113.7% and 71.2% compared to that of the basic operating cycle and the cycle with traditional mass recovery phase, respectively. The performance of the ACS with conducting the advanced mass recovery phase was better than that of conducting only the traditional mass recovery phase.

Development and Investigation of the Nano-structured Composite Surface

Enhancing the condensation rate is a key to improve the performance of the condenser. In this section, five different surfaces (plain copper plate surface, nano-structured superhydrophilic surface, nano-structured superhydrophobic surface, nano-structured superhydrophobic – zeolite 13X adsorbent composite surface and nano-structured superhydrophilic – zeolite 13X adsorbent composite surface) were developed to enhance the condensation rate in the condenser. In order to evaluate the influences of the various surfaces and operating conditions on the condensation rate, an experiment setup was designed and built.

Preparation of the nano-structured composite surfaces

The nano-structured composite surface can be coated onto an aluminum surface or copper surface. In order to make sure the surface temperature is homogeneous during the experiment and simplify the preparation and investigation, square copper plates (Qian and Shen, 2005) were selected as the substrates because of their excellent thermal conductivity (Aksan and Rose, 1973; Miljkovic and Wang, 2013) and durability (Marto et al., 1986). The nano-structured superhydrophobic surface and nano-structured superhydrophilic surface were coated onto a copper plate with a dip coating method. The complete procedure is described as follows:

1) Prepare a copper plate with a dimension of 50 mm x 50 mm x 2 mm (length x width x thickness) as a substrate.
2) Polish the copper plate with sandpaper with 100, 200, 500, 600, 800, 1000, 1200, 1500, 2000 grits in sequence to minimize the oxidation effect on the surface. After being polished with 2000-grit sandpaper, the color of the copper plate surface should look pinkish gold.
3) Immerse the polished copper plate into an acetone solution in a beaker with a volume of 100 ml for 10 minutes to degrease.
4) Take the copper plate out of the acetone solution with a pair of forceps and immerse it into the pure ethanol in a beaker for 10 minutes to remove the acetone.
5) Take the copper plate out of the pure ethanol, clean the copper plate with deionized water and dry it with compressed nitrogen.
6) Immerse the copper plate into the silver nitrate solution ($AgNO_3$) with a concentration of 0.01 mol/L in the beaker for 10 minutes. The $AgNO_3$ solution is used as a nano-coating substance. After immersion in the silver nitrate solution, the copper plate becomes black.

7) Take the copper plate out of the silver nitrate solution, clean it with deionized water and dry it with compressed nitrogen.
8) Immerse the copper plate into the 11-mercaptoundecan-1-undecano (MUD) solution with a concentration of 0.001 mol/L in a dichloromethane (CH_2Cl_2) or heptadecafluoro-1-decanethiol (HDFT) solution with a concentration of 0.001 mol/L in CH_2Cl_2 in a beaker for 15 minutes. The MUD solution and HDFT solution are used as water repellent agents. The MUD solution is used for the nano-structured superhydrophilic surface and the HDFT solution is used for the nano-structured superhydrophobic surface.
9) Take the copper plate out of the MUD/HDFT solution and immerse it into pure ethanol in a beaker for 1 minute.
10) Take the copper plate out of the pure ethanol and dry it with compressed nitrogen. The nano-structured superhydrophobic or superhydrophilic surface with a thickness of 150-300 nm (Larmour et al., 2007) is coated onto the plate.

After fabricating the nano-structured superhydrophobic surface or nano-structured superhydrophilic surface, a zeolite 13X adsorbent membrane is coated onto the nano-structured surface with an electrostatic coating method. Electrostatic coating is a coating method using a high voltage electrostatic electric field to force the particles charged negatively to move in the opposite direction of the electric field and coat the particles onto the surface. The preparation of the adsorbent membrane is shown as follows:

1) Dry the zeolite 13X adsorbent at a the temperature of 150 ^{o}C for 24 hours, powder it and then put the powder into the canister of an electrostatic sprayer which is shown in Figure 1(a);
2) Spread the binder on the area of the plate surface, which is designed for the adsorbent membrane, while the other part of the surface is covered by acrylic plates;

3) The powder in the canister is sprayed through the spray gun due to the pressure difference created by the pressure pump. The distance between the spray gun and substrate is 20 cm and the spray direction is 90 ^{o} with the substrate;
4) Remove the acrylic plates and clean the composite surface with compressed air.

A plate coated with the nano-structured superhydrophobic surface is shown in Figure 1(b) and a plate coated with the nano-structured superhydrophobic – zeolite 13X adsorbent composite surface is shown in Figure 1(c). When the thickness of the adsorbent membrane is smaller than 1 mm, the thermal resistance of the coated plate will not increase significantly compared with that of the uncoated plate (Restuccia and Cacciola, 1999). A 1 mm thickness of the adsorbent membrane was used for the coating because of the point regarding thermal resistance mentioned above. A mass of 0.4 g of the adsorbent (0.2 g adsorbent for one adsorbent membrane) was measured by a balance. The width of the adsorbent membrane was 4 mm because of the spray direction and distance between the spray gun and substrate. The width of the nano-structured superhydrophobic surface or nano-structured superhydrophilic surface between two adsorbent membranes was controlled at 16 mm to ensure the water droplets on the surface will be only affect by the adsorbent membrane close to them.

Experimental set up for the investigation of the nano-structured composite surfaces

In this study, two of the most important parameters, contact angle and condensation rate, were experimentally investigated. The contact angle was measured by a contact angle meter. The investigation of the condensation rate was conducted with an experimental setup in an environmental chamber. A schematic design of the experimental setup is shown in Figure 2.

In Figure 2, the blue line represents the water cycle. The volume of the environmental chamber is 30 m^3. The controllable ranges of temperature and relative humidity are -10 ^{o}C – 35 ^{o}C with an accuracy of ± 0.5 ^{o}C and 20 % – 95 % RH with an accuracy of ± 0.5 % RH,

respectively. The volume and power of the constant temperature bath are 15 L and 2 kW, respectively. The controllable range of temperature is -5 ^{o}C – 95 ^{o}C. Two K-type thermocouples are used to measure the water inlet and outlet temperatures to ensure the temperature uniformity of the heat exchanger and calculate the heat transfer coefficient of the composite surface. A vortex flowmeter is used to measure the water flow rate. The water is supplied from the constant temperature water bath to a plate heat exchanger to remove the condensation heat from the composite surface. A beaker is located right under the testing sample and used to collect the condensed water. An electrical balance is used to measure the weight of condensed water in the beaker. Figure 3 shows the environmental chamber, heat exchanger and other major components of the experimental setup.

A standard operating condition of the experimental setup is shown in Table 2. N_{adb} represents the number of the adsorbent membranes (adsorbent bars) coated onto the nano-structured superhydrophilic surface or nano-structured superhydrophobic surface of the composite surface. For example, N_{adb} is equal to two for the composite surface shown in Figure 1(c). RH_{ec} represents the relative humidity in the environmental chamber. T_{ec} represents the air temperature in the environmental chamber. $T_{w,in}$ and $\dot{m}_{cw}$ represent the water inlet temperature and water mass flow rate from the water bath. $W_{w,crt}$, $W_{cu,crt}$ and $W_{adb,crt}$ represent the weight of water inside the heat exchanger, the weight of the copper of the heat exchanger and plate, and the weight of adsorbent coated onto the nano-structured composite surface. Zeolite 13X is used as the coating material for the adsorbent membrane. The water temperature was measured at the water inlet and outlet of the heat exchanger, so that the energy loss from the pipe to the surroundings is negligible. Because the temperature difference between the inlet and outlet is small (e.g. less than 0.2 ^{o}C), the surface temperature is regarded as the average of the water inlet and outlet temperature. Apart from the surface contacted with the test sample of the composite surface, the other surfaces of the heat

exchanger are well insulated by heat isolation tags, so that the energy loss from the heat exchanger to the surroundings is negligible.

In order to investigate the performance of the nano-structured composite surface, different experiments under various operating conditions were conducted as shown in Table 3. In this study, the effects of the surface temperature and relative humidity in the environmental chamber on the condensation rate of the nano-structured surface were investigated. Furthermore, the effect of different patterns of adsorbent membranes on the condensation rate was also investigated experimentally.

Experimental investigation of the nano-structured composite surfaces

The contact angles of water droplets on the copper plate surface, nano-structured superhydrophilic surface, nano-structured superhydrophobic surface were measured with a contact angle meter. The contact angles in five different positions, which are shown in Figure 4 were measured. The five positions were located at the center and four corners (10 mm away from the edges) of the surface. Each position was measured three times and their average was recorded as the final result of the contact angle on each position.

In Table 4, the experimental results of the contact angles of copper plate surface, nano-structured superhydrophilic surface and nano-structured superhydrophobic surface at different positions are listed. From Table 4, it can be found that the average contact angles of the nano-structured superhydrophilic surface and nano-structured superhydrophobic surface are 3.7 ^{o} and 164.5 ^{o}, respectively. This shows that the dip coating method is practicable and the nano-structured superhydrophilic and nano-structured superhydrophobic surfaces are well prepared.

In Figure 5, the effects of the temperature of the surfaces under a relative humidity of 95%RH on the condensation rates of different surfaces, namely the copper plate surface,

nano-structured superhydrophilic surface, nano-structured superhydrophobic surface, nano-structured superhydrophilic - adsorbent composite surface and nano-structured superhydrophobic - adsorbent composite surface, are presented. From Figure 5, it can be seen that the condensation rate increases with the decrease of the surface temperature. The lower the surface temperature achieved, the larger the heat transfer between the test sample surface and moist air achieved, which led to a higher condensation rate. The condensation rates of the nano-structured superhydrophilic surface, nano-structured superhydrophobic surface, nano-structured superhydrophilic - adsorbent composite surface and nano-structured superhydrophobic - adsorbent composite surface were 37.2 g/m^2min, 41.1 g/m^2min, 48.7 g/m^2min and 49.3 g/m^2min, respectively, which show an improvement of 13.1 %, 24.8 %, 48.0 % and 49.9 %, respectively, compared with the condensation rate of the copper surface, under the operating condition of a surface temperature of 7 ^oC and a relative humidity of 95 %.

In Figure 6, the effects of the relative humidity in the environmental chamber on the condensation rates of different nano-structured surfaces with a surface temperature of 7 ^oC are shown. It can be seen that the condensation rate increases with the increase of the relative humidity. The higher the relative humidity achieved, the more water vapor in the moist air, and the larger the mass transfer from the moist air to the membrane achieved, which led to a higher condensation rate.

As illustrated in Figures 5 & 6, the nano-structured superhydrophobic surface had a better performance than the nano-structured superhydrophilic surface. In practice, the condensation performances of the surfaces rely on the distinct condensate modes, which are related to surface wettability and structure. On the nano-structured superhydrophobic surface, dropwise condensation occurs, while on the nano-structured superhydrophilic surface, filmwise condensation occurs because of the different wettability. The condensed water droplets are

easier to be removed from the nano-structured superhydrophobic surface than the nano-structured superhydrophilic surface, which leads to a reduction of the wettability and removal of the liquid film. With the reduction of the wettability and removal of the liquid film, the thermal resistance is reduced which leads to a better heat transfer performance and condensation rate.

In Figures 5 & 6, it also can be seen that the nano-structured superhydrophilic – zeolite 13X adsorbent composite surface has a better performance than the nano-structured superhydrophilic surface, and the nano-structured superhydrophobic – zeolite 13X adsorbent surface has a better performance than the nano-structured superhydrophobic surface. There may be several reasons why the composite surfaces had better performance and these are listed as follows:

1) There was a van der Waals force from the adsorbent membrane acting on the droplets on the nano-structured superhydrophilic or nano-structured superhydrophobic surfaces. The van der Waals force might affect and accelerate the movement of the droplets, so that the droplets moved towards the adsorbent membrane quickly, which could reduce the wettability of the nano-structured surface. The condensation rate increased with the reduction of the wettability. Moreover, some scattering adsorbent particles may stick to the area of the nano-structured superhydrophilic surface or nano-structured superhydrophobic surface near the adsorbent membrane. This may enlarge the effective area of the van der Waals force. More droplets could be affected, moving to the adsorbent membrane, and thus the wettability would be further reduced.
2) The droplets which were close to the adsorbent membrane moved towards the adsorbent membrane because of the van der Waals force, so that the droplets combined with other droplets on their way to form bigger droplets, which would be easier to remove from the composite surface and would reduce the wettability.

3) The van der Waals force might also affect the water vapor in the moist air, so that the humidity of the area close to the composite surface might increase, which would lead to a higher mass transfer between the nano-structured composite surface and moist air.
4) The adsorbent membrane was in a cuboid shape, which increased the total contact area between the moist air and composite surface, and it may also enlarge the effective area of the van der Waals force (Firouzi and Nguyen, 2014).

In Figure 7, the effect of the various numbers of adsorbent membranes on the composite surface on the condensation rate is shown. The results show that with the increase in the quantity of adsorbent membranes, the weight of the condensed water and the condensation rate increased. The reason was the area affected by the adsorbent membrane increased with the increase of the quantity of adsorbent membranes, which means that more droplets and water vapor were affected by the adsorbent membrane because of the van der Waals force. According to the four reasons listed above as to why the composite surfaces had better performances than the nano-structured superhydrophilic surface, nano-structured superhydrophobic surface and copper plate surface, more droplets and water vapor were affected leading to a higher condensation rate. The condensation rate of the nano-structured superhydrophilic - three adsorbent bars composite surface was 52.5 g/m^2min, which showed improvements of 19.1% and 7.8%, compared with that of the one adsorbent bar and two adsorbent bars composite surfaces, respectively. Similarly, the condensation rate of the nano-structured superhydrophobic - three adsorbent bars composite surface was 54.7 g/m^2min, which showed improvements of 18.8% and 10.9%, compared with that of the one adsorbent bar and two adsorbent bar composite surfaces, respectively. The maximum quantity of the adsorbent membranes is three because of the limitation of the size of the copper plate, while it does not mean that the optimized quantity is three. When the widths of the adsorbent membrane and the nano-structured superhydrophobic surface or

nano-structured superhydrophilic surface are reduced, the maximum quantity of the membranes which can be coated increases, which may enhance the performance of the nano-structured composite surfaces because the increase of amount of adsorbent coated onto the nano-structured composite surface. However, the condensation rate of the nano-structured composite surface may not always keep increasing with the increase in the amount of the quantity of the adsorbent membranes. If two adsorbent membranes are too close to each other, the water droplet size will be limited, which will decrease the condensation rate. Meanwhile, the water droplets between two adsorbent membranes are affected by the van der Waals forces from these adsorbent membranes which are in opposite directions, so that the influence of the adsorbent membranes on the water droplets is reduced.

As stated in this section, the condensation rate of the 50 mm x 50 mm nano-structured superhydrophobic - two adsorbent bars composite surface was 49.3 g/m^{2}min, under an operation condition of a cooling water inlet temperature of 7 ^{o}C, and a relative humidity of 95%, which shows an improvement of 50% compared with that of the copper plate surface.

In order to simulate the improvement of the cooling performance of the adsorption cooling system after utilizing the nano-structured composite surface, the overall heat transfer coefficient is required and this can be calculated based on the experimental results of the testing of the condensation rate. The energy balance equation about the testing of the condensation rate on the nano-structured composite surface can be described as follows:

$$\frac{d}{dt}[W_{w,crt}c_{p,w} + W_{cu,crt}c_{p,cu} + W_{adb,crt}c_{p,adb} + W_{adb,crt}\omega_{crt}c_{p,w})T_{con,crt}] = L_w\dot{m}_{v,crt} + \dot{m}_{v,crt}c_{p,v}(T_{ec} - T_{con,crt}) + \dot{m}_{w,crt}c_{p,w}(T_{w,crt,in} - T_{w,crt,out}), \quad (1)$$

where $W_{w,crt}$, $W_{cu,crt}$, and $W_{adb,crt}$ represent the weights of the water in the heat exchanger, the copper heat exchanger and copper plate, and the adsorbent on the nano-structured composite surface in the condensation rate testing. ω_{crt} represents the water

uptake by the adsorbent of the adsorbent membranes in the condensation rate testing. $T_{con,crt}$, T_{ec}, $T_{w,crt,in}$ and $T_{w,crt,out}$ represent the temperature of the condensation temperature on the nano-structured surface, the environmental chamber, water inlet and water outlet. $\dot{m}_{v,crt}$ and $\dot{m}_{w,crt}$ represent the condensation rate and the water flow rate. $T_{w,crt,out}$ can be expressed by:

$$T_{w,crt,out} = T_{con,crt} + \left(T_{w,crt,in} - T_{con,crt}\right)\exp\left(\frac{-U_{cs}A_{cs}}{\dot{m}_{w,crt}c_{p,w}}\right), \quad (2)$$

where U_{cs} represents the overall heat transfer coefficient of the nano-structured composite surface and the heat exchanger, A_{cs} represents the heat transfer area of the nano-structured composite surface. During the testing under the operation condition of a cooling water inlet temperature of 7 ^{o}C, and a relative humidity of 95%, an average cooling water outlet temperature of 7.12 ^{o}C was recorded and a heat transfer coefficient of 458.6 W/m^{2}K was estimated according to Eq. 1 and Eq. 2.

Error Analysis

The K-type thermocouples have an uncertainty of ± 0.1 ^{o}C. The vortex flowmeters have an uncertainty of ± 0.5%. The uncertainties of temperature and relative humidity in the environmental chamber are ± 0.5 ^{o}C and ± 0.5 %, respectively. The constant temperature water bath has an accuracy of ± 0.05 ^{o}C. The electrical balance has an accuracy of ± 0.01 g. In order to reduce the effect of errors, every single experiment was repeated three times. The average error of the experimental results of the condensation rate was estimated as ± 0.8 g/m^{2}min.

Mathematical Models

In this study, mathematical models have been developed to numerically investigate the cooling performance of the ACS as well as to evaluate the effect of using nano-structured composite surfaces in the condenser on the cooling performance of the ACS.

Assumptions

In order to develop the mathematical models, a number of assumptions are required.

1) There is no heat loss to the ambient because of the good insulation of system.
2) The temperature and pressure are uniform in the adsorbers.
3) The equilibrium water vapor uptake is uniform in the adsorbers.
4) The water vapor flows through the evaporator, and the two adsorbers and condenser are driven by pressure drop only.
5) The water vapor is an ideal gas and it becomes liquid after it is adsorbed by the adsorbent.
6) The water vapor condenses without superheat in the condenser.
7) The water evaporates without supercool in the evaporator.
8) The amount of water inside the evaporator and condenser is uniform.
9) The properties of the water, tubes and water vapor in the system are constant.
10) The thermal resistance between the copper tubes and fins of the adsorbent beds is neglected.
11) Flow resistance for water flows in tubes is neglected.
12) Effect from diffusion on the water vapor flow is neglected.

Based on these assumptions, a dynamic behavior of heat and mass transfer of the adsorption cooling system can be described as shown below.

Equilibrium Water Uptake and Adsorption Rate

In this study, silica gel is used as the adsorbent in the adsorber, while zeolite 13X is used as the adsorbent material of the composite surface in the condenser. Based on the study done by Sakoda and Suzuki, the equilibrium water uptake of silica gel can be expressed by (Sakoda and Suzuki, 1984):

$$\omega_{eq} = [P_v/P_s(T_{adb})]^{1/1.6}, \quad (3)$$

where ω_{eq} is the equilibrium amount of water uptake in the adsorbent; P_v is the water vapor pressure in the adsorber; T_{adb} is the adsorbent temperature; $P_s(T_{adb})$ is the corresponding saturated vapor pressure under the adsorbent temperature, T_{adb}. The saturated vapor pressure can be calculated by the Antoine equation (Dean and Lange, 1999):

$$\log_{10}P_s = 8.07131 - 1730.63/(T_{adb} - 39.574), \quad (4)$$

In Eq. 4, the unit of P_s is mmHg, while in other equations, the unit of pressure is Pa. During the adsorption phase, the adsorption process occurs and is controlled by surface diffusion inside the adsorbent particles. The adsorption process will stop when the water uptake reaches the equilibrium amount of water uptake. A linear driving force equation can be used to estimate the adsorption rate (Sakoda and Suzuki, 1984):

$$\frac{d\omega}{dt} = K(\omega_{eq} - \omega), \quad (5)$$

where K is the overall mass transfer coefficient which can be calculated by Eq. 6:

$$K = \frac{15D_{s0}}{r_p^2}\exp(\frac{-E_a}{RT_{adb}}), \quad (6)$$

where D_{s0} is the pre-exponent constant; r_p is the radius of the adsorbent particle; E_a is the activation energy of surface diffusion; R is the gas constant of 8.314 J/Kmol.

Energy and mass balance for the adsorber/desorber

The energy balance for the adsorber can be described by Eq. 7:

$$\frac{d}{dt}\left[\left(W_{adb}c_{p,adb} + W_{adb}\omega_{ads}c_{p,w} + W_{cu,ads}c_{p,cu} + W_{al,ads}c_{p,al}\right)T_{ads}\right]$$
$$= \Delta H W_{adb}\frac{d\omega_{ads}}{dt} + \dot{m}_{v,ads}c_{p,v}(T_{eva} - T_{ads}) + \dot{m}_{cw,ads}c_{p,w}\left(T_{cw,ads,in} - T_{cw,ads,out}\right), \quad (7)$$

where t is time; W_{adb}, $W_{cu,ads}$, $W_{al,ads}$ are the weight of the adsorbent, copper tubes, and aluminum fins in the adsorber, respectively; $c_{p,adb}$, $c_{p,w}$, $c_{p,cu}$, $c_{p,al}$, $c_{p,v}$ represent the specific heat capacity of the adsorbent, water copper, aluminum and water vapor, respectively; ω_{ads} is the water uptake in the adsorber; T_{ads}, T_{eva}, $T_{cw,ads,in}$, $T_{cw,ads,out}$, represent the temperature inside the adsorber, the temperature inside the evaporator, cooling water inlet temperature, and cooling water outlet temperature, respectively; ΔH is the adsorption heat of the adsorbent; $\dot{m}_{v,ads}$, $\dot{m}_{cw,ads}$ represent the mass flow rate of the water vapor and the cooling water in the adsorber. The cooling water outlet temperature is described as:

$$T_{cw,ads,out} = T_{ads} + \left(T_{cw,ads,in} - T_{ads}\right)\exp\left(\frac{-U_{ads}A_{ads}}{\dot{m}_{cw,ads}c_{p,w}}\right), \quad (8)$$

where U_{ads} is the heat transfer coefficient of the adsorber; A_{ads} is the heat transfer area of the adsorber. The mass flow rate of the water vapor is calculated by:

$$\dot{m}_v = \rho_v A_{pi} v_v, \quad (9)$$

where ρ_v is the density of the water vapor; A_{pi} is the cross section area of the pipes; v_v is the water vapor flow rate. The water vapor flow rate is calculated by:

$$\Delta P = \frac{1}{2}\rho_v {v_v}^2 + h_L, \tag{10}$$

where ΔP is the pressure difference; h_L is the head loss of the flow, which includes major loss, $h_{L,ma}$ and minor loss, $h_{L,mi}$. The head loss is expressed as:

$$h_L = h_{L,ma} + h_{L,mi}, \tag{11}$$

The major loss is caused by the stress force between the flow and pipe walls, which is expressed by:

$$h_{L,ma} = \frac{1}{2} f \frac{\rho_v l_{pi}}{D_{pi,i}} {v_v}^2, \tag{12}$$

where l_{pi} and $D_{pi,i}$ are the length and inner diameter of the pipes, respectively; f is the friction factor, which can be estimated by the Colebrook equation (Colebrook, 1939; Colebrook and White, 1937):

$$\frac{1}{\sqrt{f}} = -2\log\left(\frac{\lambda/D_{pi,i}}{3.7} + \frac{2.51}{Re\sqrt{f}}\right), \tag{13}$$

where λ is the equivalent roughness; Re is the Reynolds number. The minor loss is caused by valves, bends, contraction and expansion of the pipes. It can be described as:

$$h_{L,mi} = K_L \frac{1}{2}\rho_v {v_v}^2, \tag{14}$$

where K_L is the loss coefficient. From the Eq. 9-14, the mass flow rate of the water vapor can be calculated. The mass balance of the water vapor in adsorber is described as:

$$\frac{\partial(V_{adb}\varepsilon+V_{ads})\rho_{v,ads}}{\partial t} = \dot{m}_{v,ads} - V_{adb}\rho_{adb}\frac{\partial\omega_{ads}}{\partial t}, \quad (15)$$

where V_{adb} and V_{ads} represent the volume of the adsorbent and the dead volume of the adsorber, respectively; ε is the porosity of the adsorbent, $\rho_{v,ads}$ and ρ_{adb} are the density of the water vapor and adsorbent in the adsorber; $\dot{m}_{v,ads}$ is the mass flow rate of the water vapor in the adsorber; ω_{ads} is the water uptake in the adsorber. The density of the water vapor can be calculated by the ideal gas law:

$$PV = nRT, \quad (16)$$

where P is the pressure; T is the temperature. According to Eq. 16, the density of the water vapor is expressed as:

$$\rho_v = \frac{PM}{RT}, \quad (17)$$

where M is the molar mass of water. Eq. 17 is substituted into Eq. 15 and Eq. 15 becomes:

$$\frac{\partial P_{ads}}{\partial t} = \frac{RT_{ads}}{M(V_{adb}\varepsilon+V_{ads})}(\dot{m}_{v,ads} - V_{adb}\rho_{adb}\frac{\partial\omega_{ads}}{\partial t}), \quad (18)$$

where P_{ads} and T_{ads} are the pressure and temperature in the adsorber. On the other hand, the energy balance for the desorber is expressed by:

$$\frac{d}{dt}\left[\left(W_{adb}c_{p,adb} + W_{adb}\omega_{des}c_{p,w} + W_{cu,des}c_{p,cu} + W_{al,des}c_{p,al}\right)T_{des}\right]$$

$$= \Delta H W_{adb}\frac{d\omega_{des}}{dt} + \dot{m}_{hw}c_{p,w}\left(T_{hw,in} - T_{hw,out}\right), \quad (19)$$

where $W_{cu,des}$, $W_{al,des}$ are the weight of the copper tubes, and aluminum fins in the desorber, respectively; ω_{des} is the water uptake in the desorber; T_{des}, $T_{hw,in}$, $T_{hw,out}$, represent the temperature inside the desorber, hot water inlet temperature, and hot water outlet temperature, respectively; $\dot{m}_{hw}$ represents the mass flow rate of hot water in the desorber. The hot water outlet temperature is described as:

$$T_{hw,out} = T_{des} + \left(T_{hw,in} - T_{des}\right)\exp\left(\frac{-U_{des}A_{des}}{\dot{m}_{hw}c_{p,w}}\right), \quad (20)$$

where U_{des} is the heat transfer coefficient of the desorber; A_{des} is the heat transfer area of the desorber. Similar to the mass balance of the water vapor in the adsorber, that in the desorber is calculated by:

$$\frac{\partial P_{des}}{\partial t} = -\frac{RT_{des}}{M(V_{adb}\varepsilon + V_{ads})}\left(\dot{m}_{v,des} + V_{adb}\rho_{adb}\frac{\partial \omega_{des}}{\partial t}\right), \quad (21)$$

where P_{des} and T_{des} are the pressure and temperature in the desorber.

Energy and mass balance for the evaporator

The energy balance in the evaporator can be described as:

$$\frac{d}{dt}\left[\left(W_{w,eva}c_{p,w} + W_{cu,eva}c_{p,cu} + W_{al,eva}c_{p,al}\right)T_{eva}\right]$$

$$= -L_w\dot{m}_{v,ads} + \dot{m}_{v,ads}c_{p,w}(T_{con} - T_{eva}) + \dot{m}_{chw}c_{p,w}\left(T_{chw,in} - T_{chw,out}\right), \quad (22)$$

where $W_{w,eva}$, $W_{cu,eva}$, and $W_{al,eva}$ represent the weight of water, copper tubes and aluminum fins of the heat exchanger in the evaporator, respectively; L_w is the latent heat change of the water to water vapor; T_{con}, $T_{chw,in}$, and $T_{chw,out}$ represent the temperature in the condenser, chilled water inlet temperature and chilled water outlet temperature, respectively. The chilled water outlet temperature is described as:

$$T_{chw,out} = T_{eva} + \left(T_{chw,in} - T_{eva}\right)\exp\left(\frac{-U_{eva}A_{eva}}{\dot{m}_{chw}c_{p,w}}\right), \quad (23)$$

where U_{eva} is the heat transfer coefficient of the evaporator; A_{eva} is the heat transfer area of the evaporator. The mass balance of water in the evaporator is expressed by:

$$\frac{dW_{w,eva}}{dt} = -\dot{m}_{v,ads} + -\dot{m}_{v,des}, \quad (24)$$

Energy balance for the condenser

The energy balance of the condenser can be described as:

$$\frac{d}{dt}\left[\left(W_{w,con}c_{p,w} + W_{cu,con}c_{p,cu} + W_{al,con}c_{p,al} + W_{adb,con}c_{p,adb} + W_{adb,con}\omega_{con}c_{p,w}\right)T_{con}\right]$$
$$= L_w\dot{m}_{v,des} + \dot{m}_{v,des}c_{p,v}\left(T_{des} - T_{con}\right) + \dot{m}_{cw,con}c_{p,w}\left(T_{cw,con,in} - T_{cw,con,out}\right), \quad (25)$$

where $W_{w,con}$, $W_{cu,con}$, $W_{al,con}$, $W_{adb,con}$ and ω_{con} represent the weight of water, copper tubes, aluminum fins of the heat exchanger, the amount of adsorbent coated and water uptake by the adsorbent in the condenser. Without coating the nano-structured composite surface onto the fins, $W_{adb,con}$ is equal to zero. $\dot{m}_{cw,con}$ represents the mass flow rate of cooling water in the condenser; $T_{cw,con,in}$, and $T_{cw,con,out}$ represent the cooling water inlet and outlet

temperature to the condenser, respectively. The chilled water outlet temperature is expressed by:

$$T_{cw,con,out} = T_{con} + \left(T_{cw,con,in} - T_{con}\right)\exp\left(\frac{-U_{con}A_{con}}{\dot{m}_{cw,con}c_{p,w}}\right), \quad (26)$$

where U_{con} is the heat transfer coefficient of the condenser; A_{con} is the heat transfer area of the condenser.

Equation modified for the advanced mass recovery phase

In the mass recovery phase, the adsorber, desorber and condenser are connected to each other, and while the hot water continues to be supplied to the desorber, cooling water continues to be supplied to the adsorber. The mass balance equations of the mass recovery phase can be modified from Eq. 18 and Eq. 21:

$$\frac{\partial P_{des}}{\partial t} = -\frac{RT_{des}}{M(V_{adb}\varepsilon + V_{ads})}\left(\dot{m}_{mr,des,ads} + V_{adb}\rho_{adb}\frac{\partial \omega_{des}}{\partial t}\right), \quad (27)$$

and

$$\frac{\partial P_{ads}}{\partial t} = \frac{RT_{ads}}{M(V_{adb}\varepsilon + V_{ads})}\left(\dot{m}_{mr,des,ads} - \dot{m}_{mr,ads,con} + V_{adb}\rho_{adb}\frac{\partial \omega_{ads}}{\partial t}\right), \quad (28)$$

and

$$\frac{\partial P_{con}}{\partial t} = \frac{RT_{ads}}{M(V_{adb}\varepsilon + V_{ads})}\left(\dot{m}_{mr,ads,con} - \dot{m}_{mr,con}\right), \quad (29)$$

where $\dot{m}_{mr,des,ads}$, $\dot{m}_{mr,ads,con}$, and $\dot{m}_{mr,con}$ are the mass flow rate from the desorber to the adsorber, from the adsorber to the condenser and the condensation rate in the condenser

during the mass recovery phase, respectively. The energy balance equation of the adsorber can be modified from Eq. 7:

$$\frac{d}{dt}\left[\left(W_{adb}c_{p,adb} + W_{adb}\omega_{ads}c_{p,w} + W_{cu,ads}c_{p,cu} + W_{al,ads}c_{p,al}\right)T_{ads}\right]$$
$$= \Delta H W_{adb}\frac{d\omega_{ads}}{dt} + \dot{m}_{mr,des,ads}c_{p,v}(T_{des} - T_{ads}) + \dot{m}_{cw,ads}c_{p,w}\left(T_{cw,ads,in} - T_{cw,ads,out}\right), \quad (30)$$

The energy balance equation of the desorber is the same as Eq. 19, while that of the condenser can be modified from Eq. 25:

$$\frac{d}{dt}\left[\left(W_{w,con}c_{p,w} + W_{cu,con}c_{p,cu} + W_{al,con}c_{p,al} + W_{adb,con}c_{p,adb} + W_{adb,con}\omega_{con}c_{p,w}\right)T_{con}\right]$$
$$= L_w\dot{m}_{mr,con} + \dot{m}_{mr,ads,con}c_{p,v}(T_{ads} - T_{con}) + \dot{m}_{cw,con}c_{p,w}\left(T_{cw,con,in} - T_{cw,con,out}\right), \quad (31)$$

Similar to Eq. 25, $W_{adb,con}$ is equal to zero without coating the composite surface onto the fins.

Equation modified for heat recovery phase

In the heat recovery phase, the water flowing through the two adsorbers is used for recovering some heat via their temperature difference. The equations for the water outlet temperature of adsorber and desorber can be modified from Eq. 8 and Eq. 20:

$$T_{cw,ads,out} = T_{ads} + \left(T_{hw,out} - T_{ads}\right)\exp\left(\frac{-U_{ads}A_{ads}}{\dot{m}_{hr}c_{p,w}}\right), \quad (32)$$

and

$$T_{hw,out} = T_{des} + \left(T_{cw,ads,out} - T_{des}\right)\exp\left(\frac{-U_{des}A_{des}}{\dot{m}_{hr}c_{p,w}}\right), \quad (33)$$

where $\dot{m}_{hr}$ is the water mass flow rate during the heat recovery phase. The energy balance equations for the adsorber and desorber during the heat recovery phase can be modified from Eq. 7 and Eq. 19:

$$\frac{d}{dt}\left[\left(W_{adb}c_{p,adb} + W_{adb}\omega_{ads}c_{p,w} + W_{cu,ads}c_{p,cu} + W_{al,ads}c_{p,al}\right)T_{ads}\right] = \Delta H_{adb}W_{adb}\frac{d\omega_{ads}}{dt} + \dot{m}_{hr}c_{p,w}\left(T_{cw,ads,in} - T_{cw,ads,out}\right), \quad (34)$$

and

$$\frac{d}{dt}\left[\left(W_{adb}c_{p,adb} + W_{adb}\omega_{des}c_{p,w} + W_{cu,des}c_{p,cu} + W_{al,des}c_{p,al}\right)T_{des}\right] = \Delta H_{adb}W_{adb}\frac{d\omega_{des}}{dt} + \dot{m}_{hr}c_{p,w}\left(T_{hw,in} - T_{hw,out}\right), \quad (35)$$

Equation for cooling performance

The SCP and COP are the major parameters for quantifying the cooling performance of the adsorption cooling system. The SCP is expressed by:

$$\mathrm{SCP} = \frac{\dot{m}_{chw}c_{p,w}\int_0^{t_{cycle}}(T_{chw,in} - T_{chw,out})dt}{W_{adb}t_{cycle}}, \quad (36)$$

and the COP is expressed by:

$$\mathrm{COP} = \frac{\dot{m}_{chw}c_{p,w}\int_0^{t_{cycle}}(T_{chw,in} - T_{chw,out})dt}{\dot{m}_{hw}c_{p,w}\int_0^{t_{cycle}}(T_{hw,in} - T_{hw,out})dt}, \quad (37)$$

Simulation Results and Discussion

Parameter Values Adopted in the Simulation

In order to estimate how the nano-structured composite surface can improve the cooling performance of the ACS, the numerical model developed in Section 4 is used. In this section, a nano-structured superhydrophobic - adsorbent composite surface with a width of 4 mm of the adsorbent membrane and a width of 16 mm of the nano-structured superhydrophobic surface is used, which is the same as the testing sample developed in Section 3. The heat exchanger consists of 50 fins with a dimension of 40 mm × 400 mm. Therefore, a total of 2000 adsorbent membranes with a dimension of 40 mm × 4 mm can be coated in the condenser and a total of 0.32 kg of adsorbent can be coated in the condenser.

Some parameter values adopted in the simulation are measured from an ACS built in our laboratory, which are listed in Table 5. Most of the values of the parameters are directly measured from the ACS, including the heat transfer areas of different components, pipe diameters, water flow rates, water inlet temperatures, and masses of different components. However, it is difficult to directly measure the heat transfer coefficients of the adsorber, desorber, evaporator and the condenser without coating the composite surface in the ACS. Therefore, these heat transfer coefficients are estimated according to the experimental results of the ACS under different hot water inlet temperatures shown in Section 5.2 (Tso et al., 2014).

In Table 6, temperature dependent parameters including the heat capacity of the water and vapor, and the latent heat of water are listed.

From Tables 5 & 6, and the mathematical models developed above, the cooling performance of the ACS before and after utilizing the nano-structured composite surface can be numerically predicted.

Verification of the Modeling

In order to verify the modeling, an ACS was built in the laboratory in Nansha, Guangzhou and an experimental testing of the ACS was conducted. A photograph of the ACS is shown in Figure 8. The main components of the ACS were a condenser, an evaporator, two adsorbers, a chilled water tank and an overall controller. The dimension of the ACS was 1 m × 1 m × 1.5 m (length × width × height). Vehicle radiators were used as the adsorbent bed because of their lower cost and simplified assembly processes. Silica gel adsorbents were put in between the fins of the radiator. The radiators had to be covered by stainless steel metal meshes to prevent the adsorbents leaking out from the radiators. A total of 5.6 kg of silica gel could be filled into an adsorber. A SCP of 180.4 W/kg and a COP of 0.29 were achieved under an operating condition of 90 ^{o}C hot water temperature, 25 ^{o}C cooling water inlet temperature, 16 ^{o}C chilled water inlet temperature, 8 L/min hot water and cooling water flow rate, 2 L/min chilled water flow rate, 660 s adsorption/desorption phase time, 85 s mass recovery time and 50 s heat recovery time (Zhu et al., 2017). This operating condition was used as the standard operating condition in the experimental and numerical investigation of the effect of the hot water inlet temperature and cooling water inlet temperature on the cooling performance of the ACS as described in the following paragraph as well.

The hot water inlet temperature is one of the most important factors which could significantly affect the performance of the ACS. Figure 9(a) shows the effect of the hot water inlet temperature on the SCP and COP. The hot water inlet temperature has a significant influence on the SCP. The SCP was improved by 207% at the hot water inlet temperature of 95 ^{o}C compared to that at 55 ^{o}C. More water vapor could be desorbed out from the adsorber with a higher hot water inlet temperature. As a result, a larger cooling power could be produced. On the other hand, it was found that the hot water inlet temperature did not greatly affect the COP, with only a 5% difference calculated at the two extremely hot water inlet temperatures. The COP decreased slightly at the 95 ^{o}C hot water inlet temperature due to a

relatively larger heat loss occurring at the higher hot water inlet temperature. The effect of the cooling water inlet temperature on the SCP and COP was investigated and the results are shown in Figure 9(b). It was found that with a higher cooling water inlet temperature, the performance of the ACS would be lower. The SCP and COP of a 35 ^{o}C cooling water inlet temperature were respectively reduced by 9% and 4.3% compared to that of the 15 ^{o}C cooling water inlet temperature. More water vapor could be adsorbed by the adsorbent with a lower cooling water inlet temperature, which led to a higher SCP and COP. Although the cooling water inlet temperature was 35 ^{o}C, the system still had a steady and good performance. Additionally, it can be seen from Figures 9(a) and 9(b) that the simulation results with the models developed in Section 4 (curves called COP Sim. and SCP Sim.) are matched well with the experimental results (curves called COP Exp. and SCP Exp.).

The effect of adsorption/desorption phase time and mass recovery phase time before and after utilizing the nano-structured composite surface

The increase of the heat transfer coefficient of the condenser, which leads to the increase of the SCP and COP of the adsorption cooling system, may also affect the optimized operating condition of the system. In this study, the operating condition of the adsorption cooling system coated with the nano-structured composite surface was numerically optimized and a comparison between the optimized operating condition of the system before and after coating the nano-structured composite surface was made.

In Figure 10, the effects of the adsorption/desorption phase time on the cooling performance of the system before and after coating the nano-structured composite surface are shown. The simulated results show that the SCP and COP of the system coated with a nano-structured composite surface is higher than that of the system uncoated at any adsorption/desorption phase time. At the same time, the SCP of the system coated with a

nano-structured composite surface reaches the peak at an adsorption/desorption phase time of 600 s, while the SCP of the uncoated system reaches the peak at an adsorption/desorption phase time of 630 s. The difference in the optimized adsorption/desorption phase time was caused by the difference of the heat transfer coefficient in the condenser. The higher the heat transfer coefficient of the condenser, the higher the condensation rate of the condenser achieved, and the more the water vapor is condensed in the condenser. The lower the pressure in the condenser and desorber achieved when the amount of condensed water increases, the more the water vapor desorbed at the certain desorption temperature from the adsorbent. Therefore, not only do the SCP and COP increase, but the optimized adsorption/desorption phase time is shortened as well.

In Figure 11, the effects of the mass recovery time on the cooling performance of the ACS before and after coating the nano-structured composite surface are shown. In the mass recovery phase, the two adsorbers and the condenser are connected to each other. Therefore, similar to the case of the adsorption/desorption phase time, the SCP and COP of the system coated with a nano-structured composite surface is higher than that of the uncoated system at any mass recovery time. Meanwhile, the SCP of the system coated with a nano-structured composite surface reaches the peak at a mass recovery time of 70 s, while the SCP of the uncoated system reaches the peak at a mass recovery time of 85 s.

Cooling performance after utilizing the nano-structured composite surface

The optimized operation conditions of the system without coating the nano-structured composite surface in the condenser was investigated in our previous study (Zhu et al, 2017). After utilizing the nano-structured composite surfaces, the optimized operation condition of the system was changed due to a higher overall heat transfer coefficient and condensation rate in the condenser. The optimized values of the adsorption/desorption phase time and mass

recovery phase time were shortened from 660 s and 85 s to 600 s and 70 s, respectively. An optimized condition was achieved with a hot water inlet temperature of 95 ^{o}C, a cooling water inlet temperature of 25 ^{o}C, a chilled water inlet temperature of 16 ^{o}C, a hot water mass flow rate of 8 L/min, a cooling water mass flow rate of 8 L/min, a chilled water mass flow rate of 2 L/min, an adsorption/desorption phase time of 600 s, a mass recovery phase time of 70 s, and a heat recovery phase time of 50 s, after utilizing the nano-structured composite surface.

Table 7 shows a comparison of the simulated SCP and COP of the ACS before and after utilizing the nano-structured composite surface in the condenser. The simulated results showed that the SCP and COP of the system coated with the nano-structured composite surface improved by 16.1% and 5.1%, respectively compared with that uncoated with the nano-structured composite surface under the same operating condition, which was the optimized operating condition of the system without coating the nano-structured composite surface shown in Table 7. After the optimization of the operating condition, a SCP of 231.4 W/kg and a COP of 0.317 were estimated, which showed an improvement of 25.0 % and 7.8 %, respectively compared with that of the system without coating the nano-structured composite surface. This shows that the performance of the condenser significantly affects the cooling performance of the ACS. Moreover, the enhancement of the performance of the condenser can shorten the optimized cycle time, which leads to a more steady cooling effect.

Figure 12 shows the simulated temperature profiles of the heat transfer fluid at different locations of the adsorption cooling system coated with the nano-structured composite surface in the condenser under the optimized operating condition. The hot water outlet temperature decreases slightly at the beginning of mass recovery phase. This is because of the desorption process in the desorber due to the reduction of pressure. The hot water outlet temperature decreases rapidly, while the cooing water outlet temperature from the adsorber increases

rapidly in the heat recovery phase. The chilled water outlet temperature is always below the chilled water inlet temperature, which means the adsorption cooling system coated with the nano-structured composite surface in the condenser can continuously produce a cooling effect.

Conclusions

In this study, an advanced mass recovery phase is conducted and investigated, a number of different surfaces, named as a copper plate surface, nano-structured nano-structured superhydrophilic surface, nano-structured nano-structured superhydrophobic surface, nano-structured superhydrophilic – zeolite 13X composite surface, and nano-structured superhydrophobic – zeolite 13X composite surface are developed. The effects of the different composite surfaces; surface temperature, relative humidity in the environmental chamber, and different patterns of the adsorbent membranes on the condensation rate are experimentally investigated. Moreover, the cooling performance of the ACS utilizing the nano-structured composite surface in the condenser is numerically investigated and compared with that without coating the composite surface. The following conclusions are drawn:

1) After conducting the advanced mass recovery phase, the SCP of the ACS increases by 113.7% and 71.2% respectively compared to that of the basic operating cycle and traditional mass recovery phase.
2) The lower the surface temperature, the higher the condensation rate achieves. Similarly, the higher the relative humidity in the environmental chamber, the higher the condensation rate achieves. Under the operating condition of a surface temperature of 7 ^{o}C and a relative humidity of 95 %RH, the condensation rates of the nano-structured superhydrophobic – zeolite 13X composite surface is 49.3 g/m^{2}min, which shows an improvement of 49.9 %, compared with that of the copper surface.

3) With the increase of the quantity of adsorbent membrane, the condensation rates of the nano-structured composite surfaces increases. The condensation rate of the nano-structured superhydrophobic - three adsorbent bars composite surface is 54.7 g/m^2min, which shows an improvement of 18.8%, compared with that of the one adsorbent bar composite surface.

4) After utilizing the nano-structured composite surface in the condenser of an ACS, a SCP of 231.4 W/kg and a COP of 0.317 are estimated, which shows an improvement of 25.0 % and 7.8 %, respectively, compared with that of the system without coating the nano-structured composite surface.

Although the results show that the nano-structured composite surfaces offer great application potential for energy saving and cooling performance enhancement in the condenser of the ACS, it should be noted that these nano-structured composite surfaces can also be applied in other thermal energy systems, such as conventional heating, ventilation, and air conditioning systems, refrigerators, dehumidifiers, adsorption desalination systems, passive radiative cooling and self-cleaning smart windows.

Different nano-structured composite surfaces are developed, and some experimental and numerical results are estimated, but the full picture of the performance of the nano-structured composite surfaces utilized in the condenser of the ACS has not been fully developed yet. In the future, the effect of the width of the adsorbent membranes and the width of the nano-structured superhydrophobic surface on the condensation rate of the nano-structured composite surfaces should be investigated. The effect of the adsorbent membranes, which consists of different adsorbent materials, on the condensation rate of the nano-structured composite surfaces should be also investigated. Moreover, numerical models should be developed and verified to describe the condensation behaviors of the water droplets, which

includes droplet formation, droplet growth, and droplet movement on the nano-structured composite surfaces.

References

Ahmed A., M. Salem, I.M. Ismael, A.H.H. Ali, M.G. Morsy, and B.B. Saha. 2012. An overview on adsorption pairs for cooling. *Renewable and Sustainable Energy Reviews* 19:565-72.

Akahira A., K.C.A. Alam, Y. Hamamoto, A. Akisawa, and T. Kashiwagi. 2004. Mass recovery adsorption refrigeration cycle-improving cooling capacity. *International Journal of Refrigeration* 27:225-34.

Aksan S.N., and J.W. Rose. 1973. Dropwise condensation-The effect of thermal properties of the condenser material. *International Journal of Refrigeration* 16(2):461-7.

Anyanwu E.E.. 2004. Review of solid adsorption solar refrigeration II: An overview of the principles and theory. *Energy Conversion and Management* 45:1279-95.

Boelman E.C., B.B. Saha, and T. Kashiwagi. 1995. Experimental investigation of a silica gel –water adsorption refrigeration cycle – The influence of operating conditions on cooling output and COP. *ASHRAE Transactions: Research* 101:358-66.

Chan K.C., C.Y. Tso, C.Y.H. Chao, and C.L. Wu. 2015. Experiment verified simulation study of the operating sequences on the performance of adsorption cooling system. *Building Simulation* 8(3):255-69.

Chua H.T., K.C. Ng, A. Malek, T. Kashiwagi, A. Akisawa, and B.B. Saha. 2002. Regenerative adsorption process and multi-reactor regenerative adsorption chiller. USA, US2002053217.

Cheng Y.P., J.L. Xu, and Y. Sui. 2016. Numerical investigation of coalescence-induced droplet jumping on superhydrophobic surfaces for efficient dropwise condensation heat transfer. *International Journal of Heat and Mass Transfer* 95:506-16.

Colebrook C.F.. 1939. Turbulent flow in pipes, with particular reference to the transition region between the smooth and rough pipe laws. *Journal of the ICE* 11(4):133-56.

Colebrook C.F., and C.M. White. 1937. Experiments with fluid friction in roughened pipes. *Proceedings of the Royal Society of London, Series A* 161(906):367-81.

Dean J.A., and N.A. Lange. 1999. Lange's handbook of chemistry, New York: McGraw-Hill.

Dong C.S., L. Lu, and T. Wen. 2017. Experimental study on dehumidification performance enhancement by TiO_2 superhydrophilic coating for liquid desiccant plate dehumidifiers. *Building and Environment* 124:219-31.

Edwards J.A., and J.S. Doolittle. 1965. Tetrafluoroethylene promoted dropwise condensation. *International Journal of Heat and Mass Transfer* 8(4):663-6.

Firouzi M., and A.V. Nguyen. 2014. On the effect of van der Waals attractions on critical salt concentration for inhibiting bubble coalescence. *Minerals Engineering* 58:108-12.

Frazzica A., G. Fuldner, A. Sapienza, A. Freni, and L. Schnabel. 2014. Experimental and theoretical analysis of the kinetic performance of an adsorbent coating composition for use in adsorption chillers and heat pumps. *Applied Thermal Engineering* 73:1022-31.

Grzech A., J. Yang, P.J. Glazer, and T.J. Dingemans. 2014. Effect of long rage van der Waals interactions on hydrogen storage capacity and heat of adsorption in large pore silicas. *International Journal of Hydrogen Energy* 39:4367-72.

Larmour I.A., S.E. Bell, G.C. Saunders. 2007. Remarkably simple fabrication of superhydrophobic surfaces using electroless galvanic deposition. *Angewandte Chemie* 119:1740-2.

Lennard-Jones J.E.. 1932. Processes of adsorption and diffusion on solid surfaces. *Transactions of the Faraday Society* 28(3):333-59.

Li T.X., R.Z. Wang, J.K. Kiplagat, L.W. Wang, and R.G. Oliveira. 2009. A conceptual design and performance analysis of a triple-effect solid-gas thermochemical sorption refrigeration system with internal heat recovery. *Chemical Engineering Science* 64:3376-84.

Li X.H., X.H. Hou, X. Zhang, and Z.X. Yuan. 2015. A review on development of adsorption cooling-Novel beds and advanced cycles. *Energy Conversion and Management* 94:221-32.

Lu M.C., C.C. Lin, W.C. Lo, C.W. Huang, and C.C. Wang. 2017. Superhydrophobic Si nanowires for enhanced condensation heat transfer. *International Journal of Heat and Mass Transfer* 111:614-23.

Luo Y.F., J. Zhu, Y.L. Ma, and H. Zhang. 2008. Dry coating, a novel coating technology for solid pharmaceutical dosage forms. *International Journal of Pharmaceutics* 358:16-22.

Marto P.J., D.J. Looney, J.W. Rose, and A.S. Wanniarachchi. 1986. Evaluation of organic coatings for the promotion of dropwise condensation of steam. *International Journal of Heat and Mass Transfer* 29(8):1109-17.

Miljkovic N., and E.N. Wang. 2013. Condensation heat transfer on superhydrophobic surfaces. *MRS Bulletin* 38(5):397-406.

Miyazaki T., A. Akisawa, and B.B. Saha. 2010. The performance analysis of a novel dual evaporator type three-bed adsorption chiller. *International Journal of Refrigeration* 33:276-85.

Ng K.C., K. Thu, B.B. Saha, and A. Chakraborty. 2012. Study on a waste heat-driven adsorption cooling cum desalination cycle. *International Journal of Refrigeration* 35:685-93.

Nidal H., A. Hamdeh, and M.A. Al-Muhtaseb. 2010. Optimization of solar adsorption refrigeration system using experimental and statistical techniques. *Energy Conversion and Management* 51:1610-5.

Prasad L.K., J.W. McGinity, and R.O. Williams III. 2016. Electrostatic powder coating: Principles and pharmaceutical applications. *International Journal of Pharmaceutics* 505:289-302.

Qi R.H., Y. Hu, Y.H. Wang, and L. Lu. 2016. A new approach to enhance the heat and mass transfer of liquid desiccant dehumidification with a titanium dioxide superhydrophilic self-cleaning coating. *Journal of Cleaner Production* 112(4):3555-61.

Qian B., and Z. Shen. 2005. Fabrication of superhydrophobic surfaces by dislocation-selective chemical etching on aluminum, copper, and zinc substrates. *Langmuir* 21(20):9007-9.

Qu T.F., R.Z. Wang, and W. Wang. 2001. Study on heat and mass recovery in adsorption refrigeration cycles. *Applied Thermal Engineering* 21:439-52.

Restuccia G., and G. Cacciola. 1999. Performance of adsorption systems for ambient heating and air conditioning. *International Journal of Refrigeration* 22(1):18-26.

Sakoda A., and M. Suzuki. 1984. Fundamental study of solar powered adsorption cooling system. *Journal of Chemical Engineering of Japan* 17:52-7.

Sapienza A., S. Santamaria, A. Frazzic, and A. Freni. 2011. Influence of the management strategy and operating conditions on the performance of an adsorption chiller. *Energy* 36:5532-8.

Sun Z., X. Chen, and H. Qiu. 2014. Experimental investigation of a novel asymmetric heat spreader with nanostructure surfaces. *Experimental Thermal and Fluid Science* 52:197-204.

Thu K., B.B. Saha, A. Chakraborty, W.G. Chun, and K.C. Ng. 2011. Study on an advanced adsorption desalination cycle with evaporator-condenser heat recovery circuit. *International Journal of Heat and Mass Transfer* 54:43-51.

Traipattanakul B., C.Y. Tso, and C.Y.H. Chao. 2017. Study of jumping water droplets on superhydrophobic surfaces with electric fields. *International Journal of Heat and Mass Transfer* 115:672-81.

Tso C.Y., C.Y.H. Chao, and S.C. Fu. 2012. Performance analysis of a waste heat driven activated carbon based composite adsorbent – water adsorption chiller using simulation model. *International Journal of Heat and Mass Transfer* 55:7596-610.

Tso C.Y., K.C. Chan, C.Y.H. Chao, and C.L. Wu. 2015. Experimental performance analysis on an adsorption cooling system using zeolite 13X/$CaCl_2$ adsorbent with various operation sequences. *International Journal of Heat and Mass Transfer* 85:343-55.

Tso C.Y., S.C. Fu, and C.Y.H. Chao. 2014. Modeling a solar-powered double bed novel composite adsorbent (silica activated carbon/$CaCl_2$) – water adsorption chiller. *Building Simulation* 7:185-96.

Wang D.C., Y.H. Li, D. Li, Y.Z. Xia, and J.P. Zhang. 2009. A review on adsorption refrigeration technology and adsorption deterioration in physical adsorption systems. *Renewable and Sustainable Energy Reviews* 14:344-53.

Wang Q., X. Gao, J.Y. Xu, A.S. Maiga, and G.M. Chen. 2012. Experimental investigation on a fluidized-bed adsorber/desorber for the adsorption refrigeration system. *International Journal of Refrigeration* 35:694-700.

Wang R.Z.. 2001. Adsorption refrigeration research in Shanghai Jiao Tong University. *Renewable and Sustainable Energy Reviews* 5:1-37.

Yang Q.L., Y.L. Ma, J. Zhu, K. Chow, and K.Q. Shi. 2017. An update on electrostatic powder coating for pharmaceuticals. *Particuology* 31:1-7.

Youssef P.G., R.K. AL-Dadah, S.M. Mahmoud, H.J. Dakkama, and A. Elsayed. 2015. Effect of evaporator and condenser temperatures on the performance of adsorption desalination cooling cycle. *Energy Procedia* 75:1464-9.

Youssef P.G., S.M. Mahmoud, and R.K. AL-Dadah. 2016. Numerical simulation of combined adsorption desalination and cooling cycles with integrated evaporator/condenser. *Desalination* 392:14-24.

Zhu L.Q., C.Y. Tso, K.C. Chan, C.L. Wu, C.Y.H. Chao, J. Chen, W. He, and S.W. Luo. 2018. Experimental investigation on composite adsorbent – water pair for a solar-powered adsorption cooling system. *Applied Thermal Engineering* 131:649-59.

Zhu L.Q., C.Y. Tso, W. He, C.L. Wu, and C.Y.H. Chao. 2017. A field investigation of a solar-powered adsorption cooling system under Guangzhou's climate with various numbers of heat exchangers in the adsorbers. *Science and Technology for the Built Environment*, 23:1282-92.

Acknowledgements

Funding sources for this research are provided by the Hong Kong Research Grant Council via General Research Fund account of 16202517, Collaborative Research Fund (CRF) account of C6022-16G, Guangzhou Science and Technology Program via account of 201807010097, and Science and Technology Program of Nansha District via account of 2016CX013.

Figure Captions

Figure 1: An electrostatic sprayer (a), a plate coated with a nano-structured superhydropbobic surface (b), a plate coated with a nano-structured superhydrophobic – zeolite 13X adsorbent composite surface (c)

Figure 2: Schematic design of the experimental setup (B = Balance, F = Water flow meter, H = Humidity meter, P = Pump, T = Thermocouple, V = Valve)

Figure 3: The environmental chamber (a), the heat exchanger (b), the experimental setup (c)

Figure 4: Five measured positions on the copper plate surface, nano-structured superhydrophilic surface and nano-structured superhydrophobic surface

Figure 5: Effect of the surface temperature on the condensation rate of different surfaces

Figure 6: The effect of the relative humidity on the condensation rate of various surfaces

Figure 7: The effect of the number of adsorbent membranes on the condensation rate of nano-structured superhydrophilic - adsorbent composite surfaces (a) and nano-structured superhydrophobic - adsorbent composite surfaces (b)

Figure 8: The adsorption cooling system

Figure 9: A comparison of the SCP and COP among the experimental results and simulation results under different hot water inlet temperatures (a) and different cooling water inlet temperatures (b)

Figure 10: The effect of the adsorption/desorption phase time on the cooling performance with and without coating the nano-structured composite surface

Figure 11: The effect of the mass recovery time on the cooling performance with and without coating the nano-structured composite surface

Figure 12: Simulated temperature profiles of heat transfer fluid

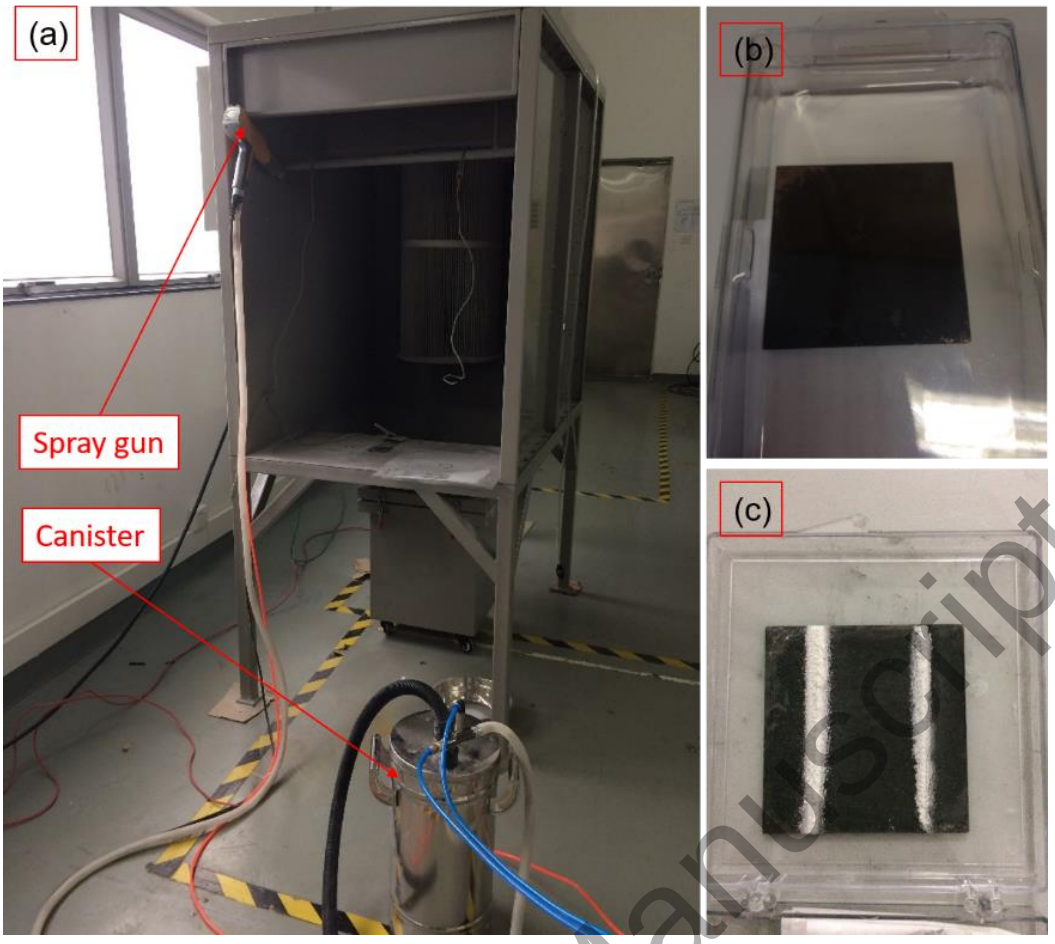

Figure 1. An electrostatic sprayer (a), a plate coated with a nano-structured superhydropbobic surface (b), a plate coated with a nano-structured superhydrophobic – zeolite 13X adsorbent composite surface (c)

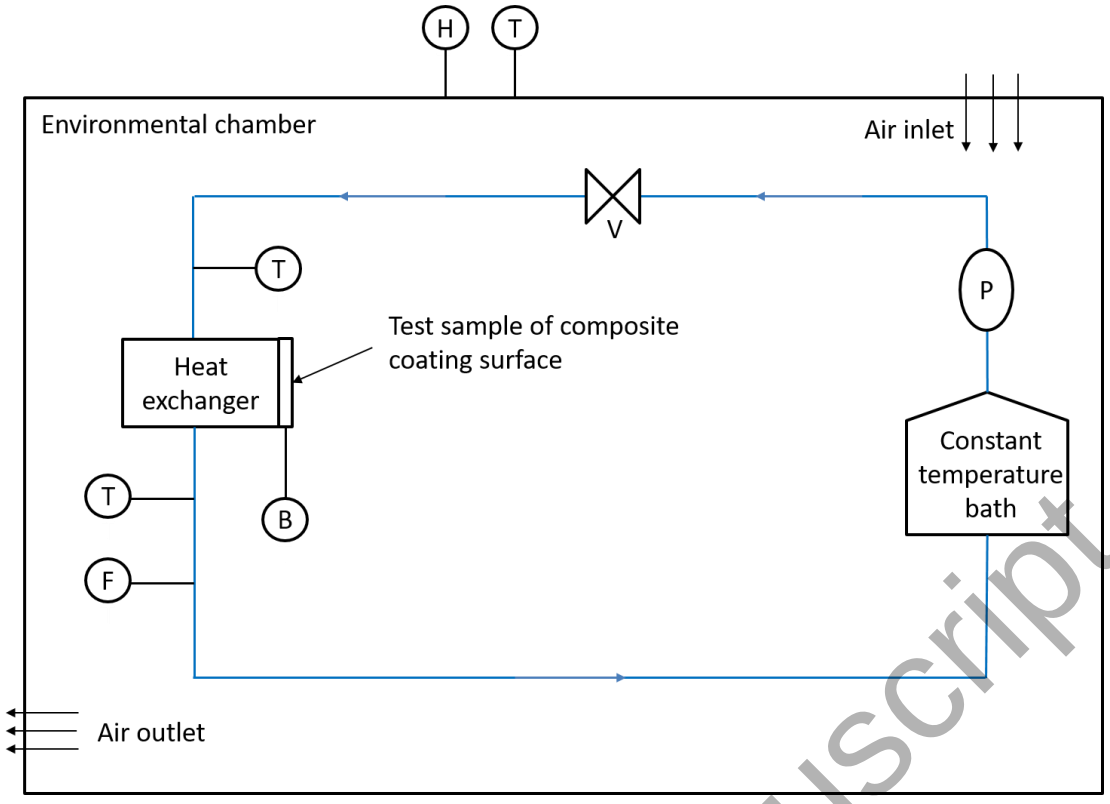

Figure 2. Schematic design of the experimental setup (B = Balance, F = Water flow meter, H = Humidity meter, P = Pump, T = Thermocouple, V = Valve)

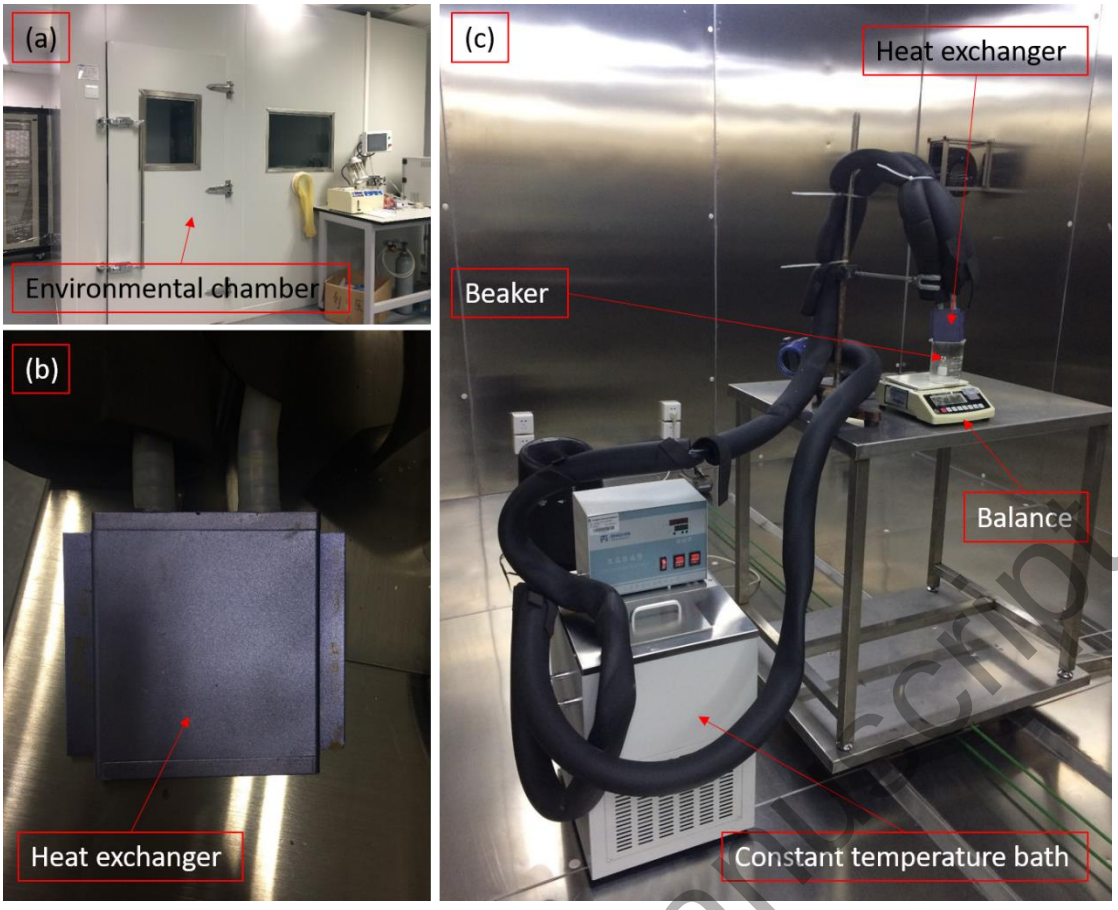

Figure 3. The environmental chamber (a), the heat exchanger (b), the experimental setup (c)

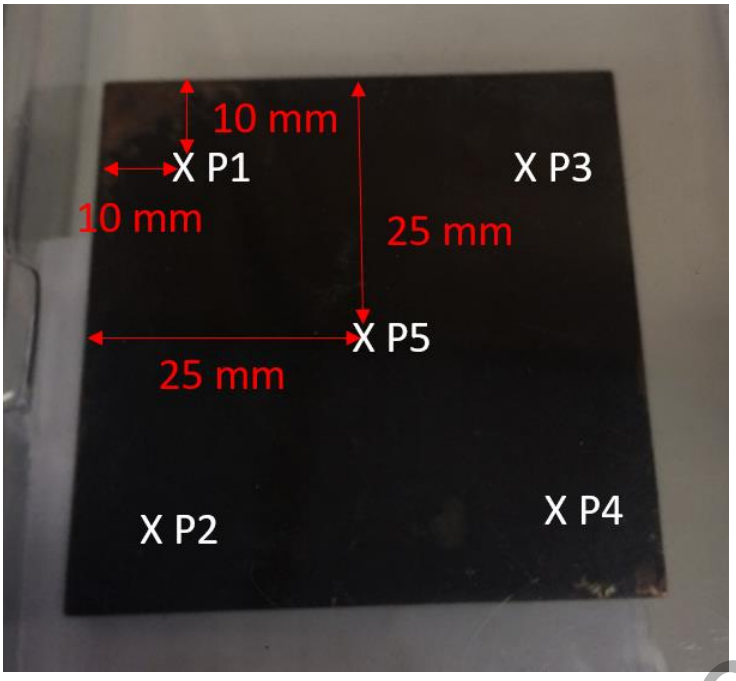

Figure 4. Five measured positions on the copper plate surface, nano-structured superhydrophilic surface and nano-structured superhydrophobic surface

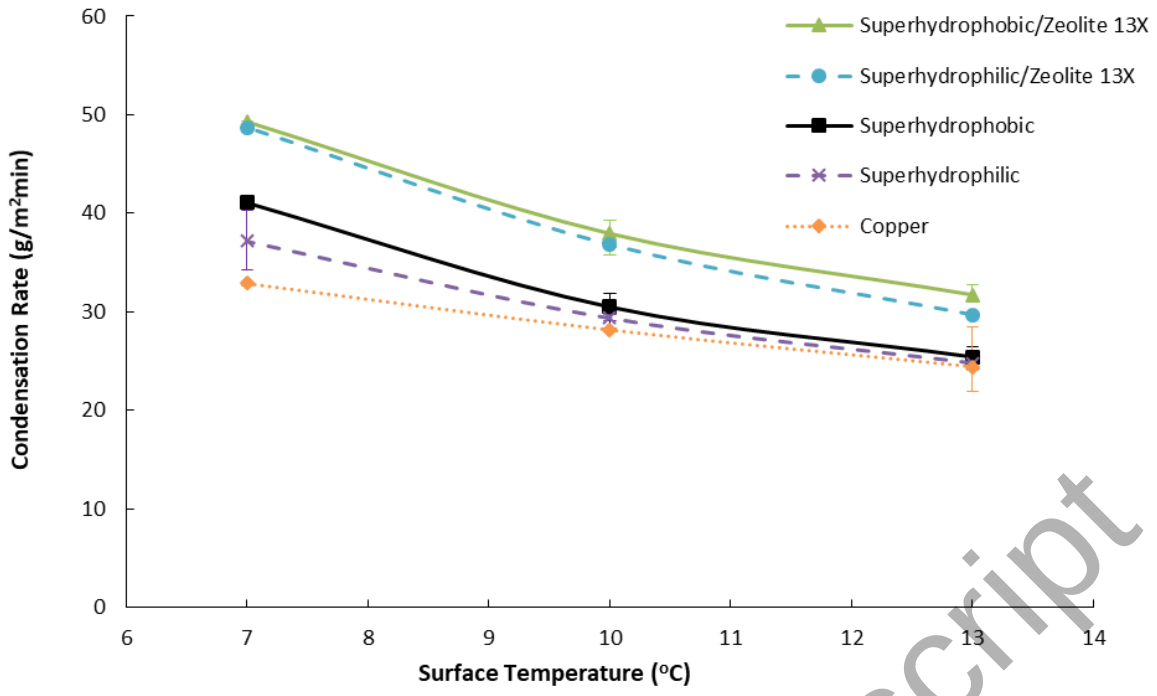

Figure 5. Effect of the surface temperature on the condensation rate of different surfaces

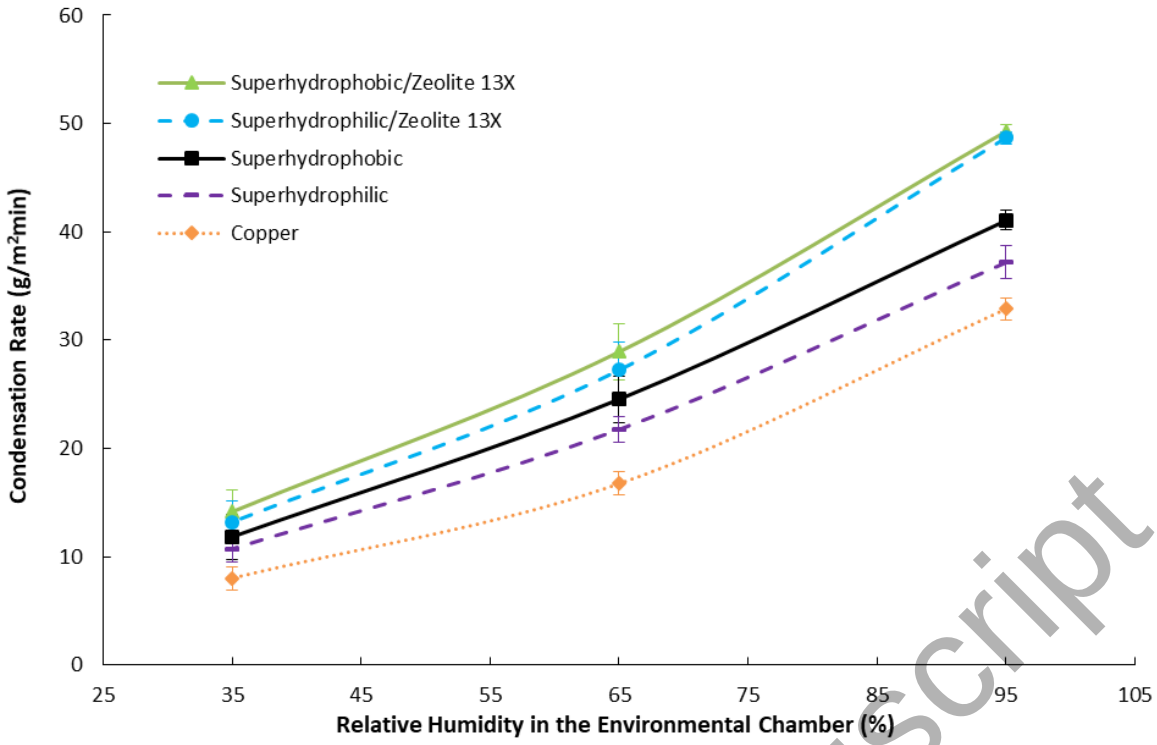

Figure 6. The effect of the relative humidity on the condensation rate of various surfaces

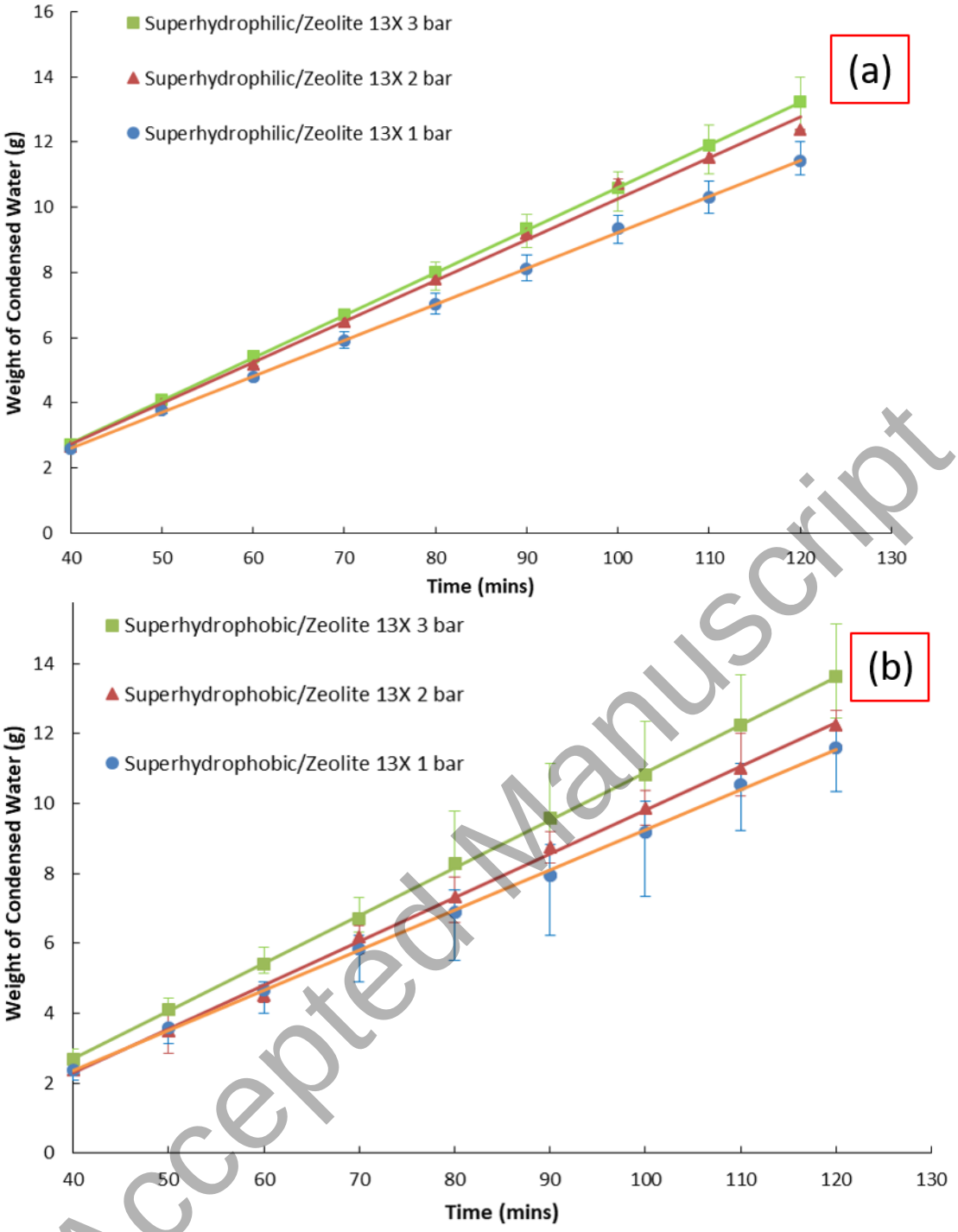

Figure 7. The effect of the number of adsorbent membranes on the condensation rate of nano-structured superhydrophilic - adsorbent composite surfaces (a) and nano-structured superhydrophobic - adsorbent composite surfaces (b)

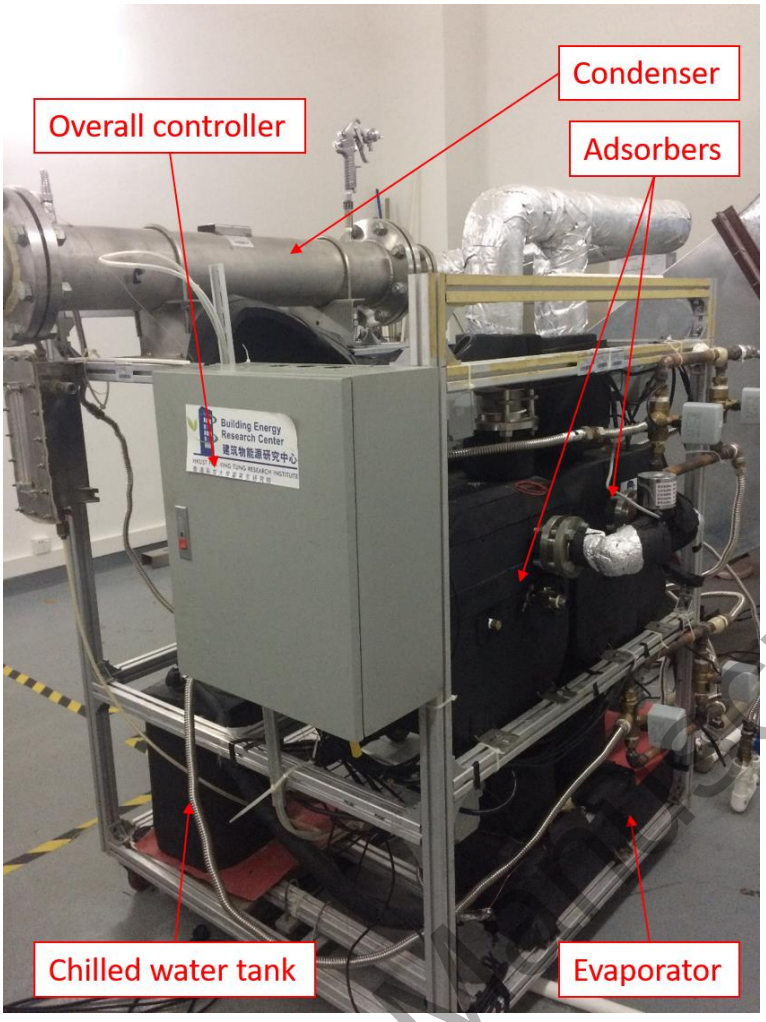

Figure 8. The adsorption cooling system

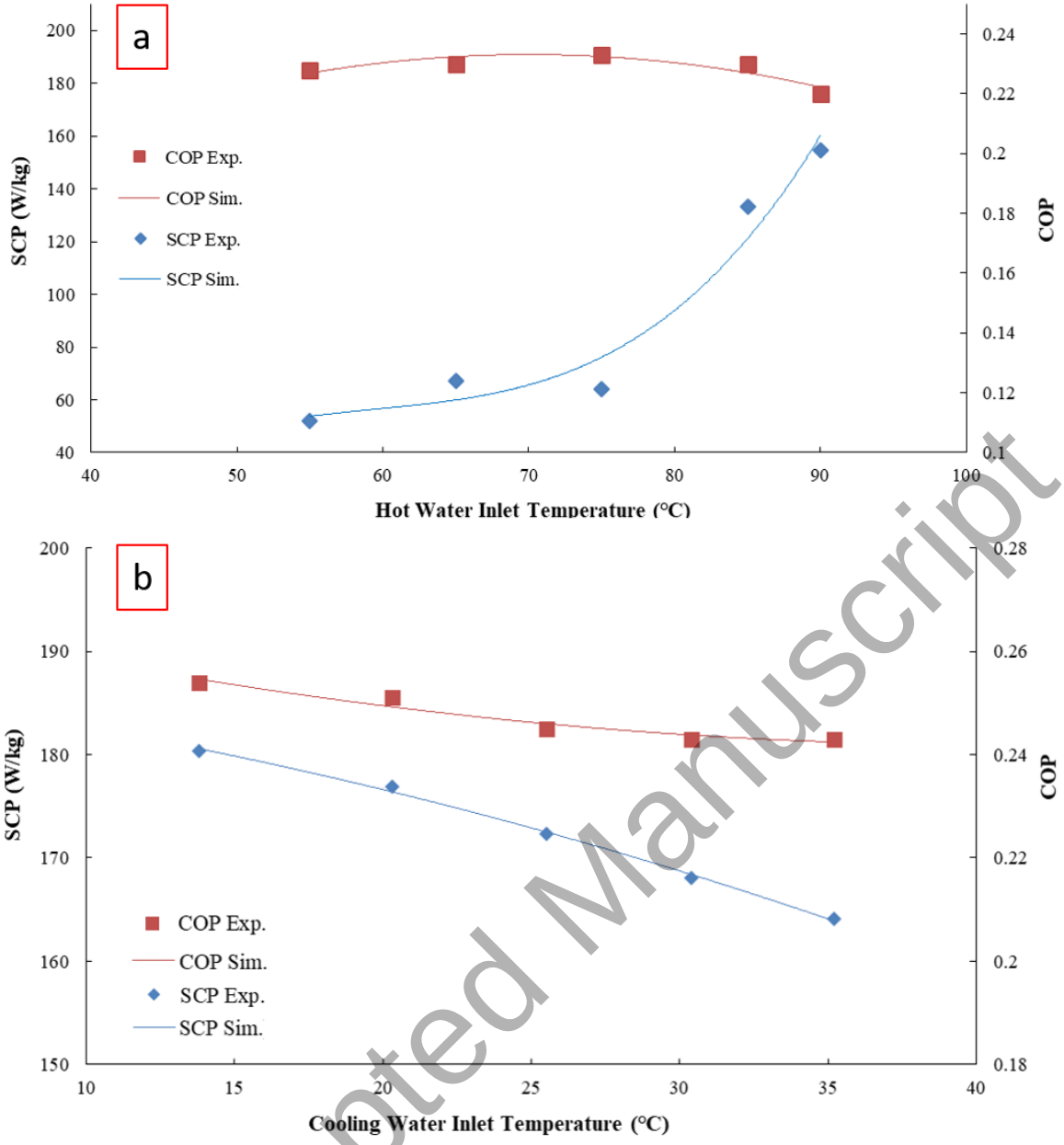

Figure 9. A comparison of the SCP and COP among the experimental results and simulation results under different hot water inlet temperatures (a) and different cooling water inlet temperatures (b)

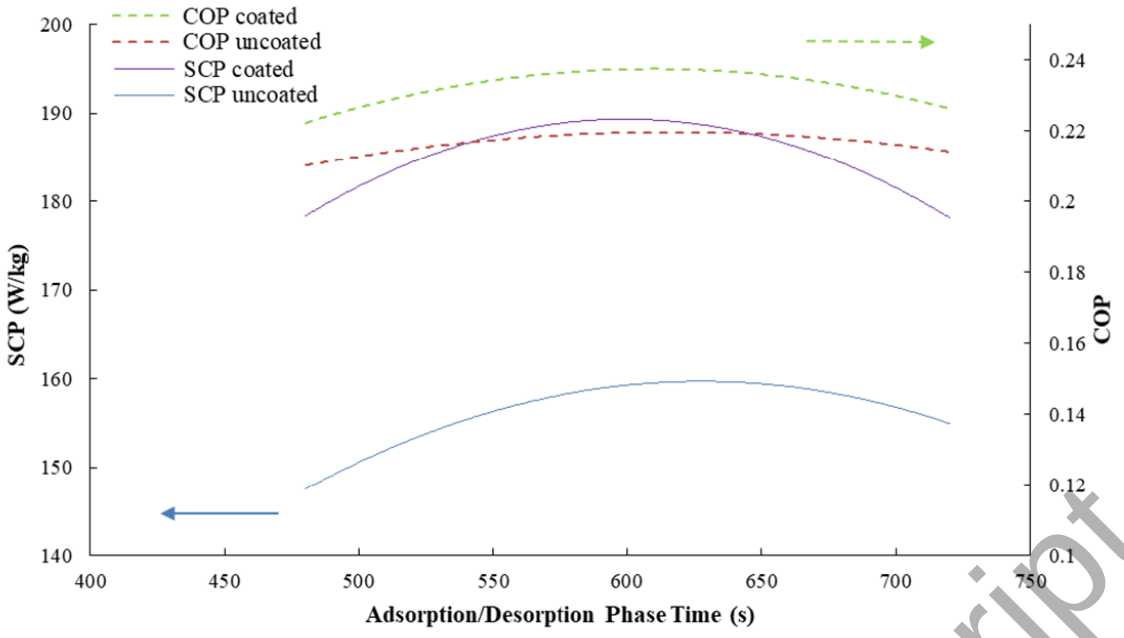

Figure 10. The effect of the adsorption/desorption phase time on the cooling performance with and without coating the nano-structured composite surface

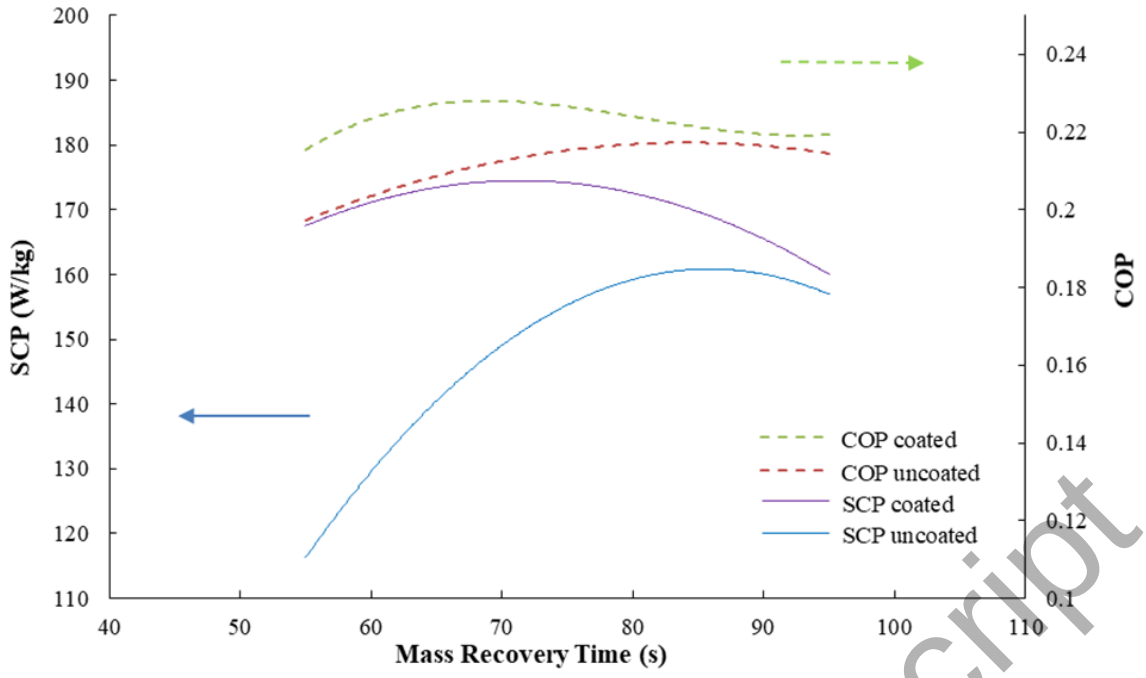

Figure 11. The effect of the mass recovery time on the cooling performance with and without coating the nano-structured composite surface

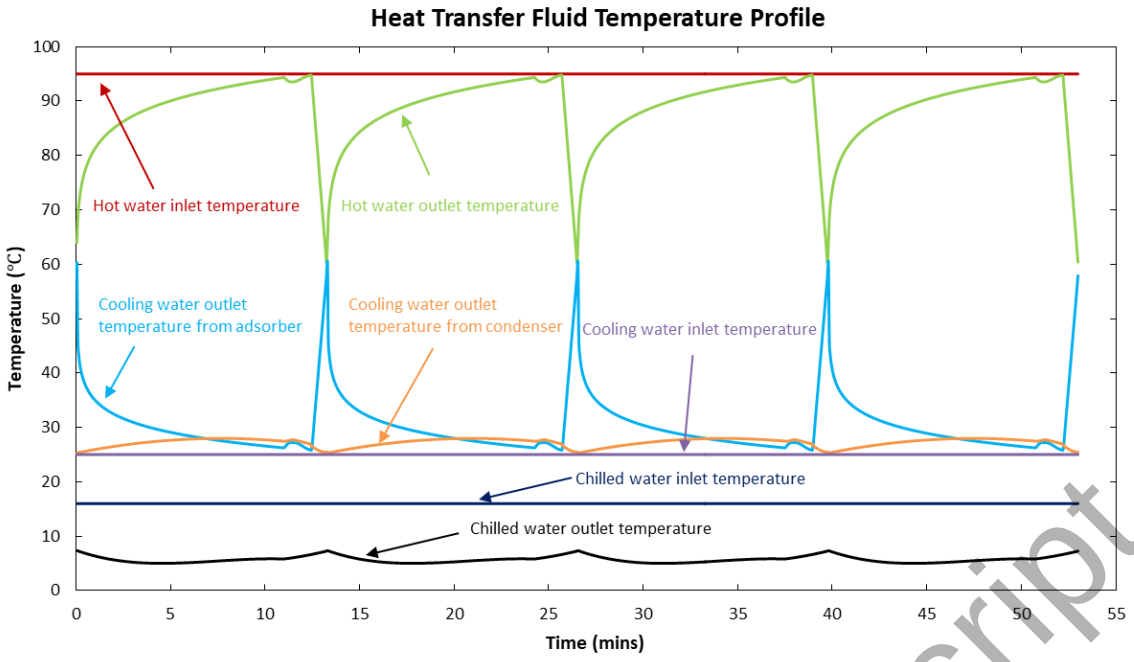

Figure 12. Simulated temperature profiles of heat transfer fluid

Table Captions

Table 1: A comparison of different operating sequences

Table 2: Standard operating condition of the experiment

Table 3: Various operating conditions

Table 4: Contact angles of the copper plate surface, nano-structured superhydrophilic surface and nano-structured superhydrophobic surface

Table 5: Parameter values adopted in the simulation

Table 6: Temperature dependent parameters adopted in the simulation

Table 7: A comparison of the cooling performance before and after utilizing the nano-structured composite surface

Table 1. A comparison of different operating sequences				
Operating Sequences	**SCP (W/kg)**	**SCP Improvement (%)**	**COP**	**COP Improvement (%)**
BC	84.4	N.A.	0.13	N.A.
BC + TMR + HR	105.4	24.9%	0.28	115.4%
BC + AMR + HR	180.4	113.7% (compared to BC) & 71.2% (compared to BC +TMR + HR)	0.25	82.3% (compared to BC)

Table 2. Standard operating condition of the experiment		
Parameters	**Values**	**Unit**
A_{cs}	2.7 x 10^{-4}	m^2
RH_{ec}	95	%
$\dot{m}_{w,crt}$	1	L/min
N_{adb}	2	N.A.
$T_{w,crt,in}$	7	^oC
T_{ec}	22	^oC
$W_{w,crt}$	12.7	g
$W_{cu,crt}$	65.9	g
$W_{adb,crt}$	0.4	g

Table 3. Various operating conditions		
Parameters	**Values**	**Unit**
N_{adb}	1, 3	N.A.
RH_{ec}	35, 65	%
$T_{w,in}$	10, 13	°C

Table 4. Contact angles of the copper plate surface, nano-structured superhydrophilic surface and nano-structured superhydrophobic surface

Position	Copper surface	Nano-structured Superhydrophilic surface	Nano-structured Superhydrophobic surface
1	80.3	3.1	166.1
2	77.6	4.1	162.3
3	80.1	4.4	165.3
4	79.3	3.5	164.7
5	78.3	3.4	163.9
Average	79.1	3.7	164.5

Table 5. Parameter values adopted in the simulation

Symbol	Value	Unit	Symbol	Value	Unit
$A_{ads,des}$	9.6	m^2	$T_{cw,in}$	25	^oC
$A_{con,uc}$	1.8	m^2	$T_{hw,in}$	95	^oC
$A_{con,c}$	1.96	m^2	U_{ads}	187.6	W/m^2K
A_{eva}	1.2	m^2	$U_{con,uc}$	259.3	W/m^2K
A_p	$5.06x10^{-4}$	m^2	$U_{con,c}$	458.6	W/m^2K
$c_{p,adb}$	924	J/kgK	U_{des}	193.9	W/m^2K
$c_{p,al}$	880	J/kgK	U_{eva}	293.1	W/m^2K
$c_{p,cu}$	386	J/kgK	V_{adb}	$9.2x10^{-3}$	m^3
ΔH	$2.8x10^6$	J/kg	V_{ads}	$5.53x10^{-2}$	m^3
$D_{p,i}$	25.4	mm	$W_{adb,ads,des}$	7	kg
D_{s0}	$2.54x10^{-4}$	m^2/s	$W_{adb,con}$	0.26	kg
E_a	$4.2x10^4$	J/mol	$W_{al,ads,des}$	2.34	Kg
l_p	26	m	$W_{al,con}$	0.89	kg
$\dot{m}_{chw}$	2	L/min	$W_{al,eva}$	0.59	kg
$\dot{m}_{cw}$	8	L/min	$W_{cu,ads,des}$	2.46	kg
$\dot{m}_{hr}$	2	L/min	$W_{cu,con}$	0.93	Kg
$\dot{m}_{hw}$	8	L/min	$W_{cu,eva}$	0.62	Kg

$\dot{m}_{mr}$	8	L/min	$W_{w,con}$	1	kg
r_{pi}	0.154	mm	$W_{w,eva}$	15	kg
t_{cycle}	1590	s	ρ_{adb}	870	kg/m^3
$T_{chw,in}$	16	^{o}C	ε	0.3	-

Table 6. Temperature dependent parameters adopted in the simulation

Symbol	Value	Unit
$c_{p,v}$	$1.1883x10^{-4}T^3$-$0.101485T^2$+30.0268T-1168.47	J/kgK
$c_{p,w}$	$-1.27742x10^{-4}T^3$+$0.134933T^2$-46.8724T+9548.13	J/kgK
L_w	$-1.23188T^2$-1629.73T+$3.03683x10^6$	J/kg

Table 7. A comparison of the cooling performance before and after utilizing the nano-structured composite surface

Adsorption cooling system	SCP (W/kg)	COP
Uncoated	185.1	0.294
Coated (under the same operating condition as the uncoated one)	215.9	0.309
Coated (under optimized operating condition)	231.4	0.317